SATELLITE-BASED ASSESSMENTS OF OCEAN ACIDIFICATION FOR THE HAWAIIAN ISLANDS REGION

A THESIS SUBMITTED TO THE GRADUATE DIVISION OF THE UNIVERSITY OF HAWAII AT MANOA IN PARTIAL FULFILLMENT OF THE REQUIREMENTS FOR THE DEGREE OF

MASTER OF SCIENCE

IN

OCEANOGRAPHY

AUGUST 2023

By
Caroline E. Jackson

Thesis Committee:
Christopher Sabine, Chairperson
Angelicque White
James Potemra

Keywords: Ocean acidification, empirical algorithms, satellite measurements, Hawaiian Islands

ACKNOWLEDGEMENTS

I would like to acknowledge and thank my Thesis Advisor, Dr. Christopher Sabine, for all of his support, guidance and feedback throughout the years and for making this research experience possible. I am very grateful to have been afforded an opportunity to pursue this area of research. I would also like to thank my Thesis Committee members, Dr. Angelicque White and Dr. James Potemra, for their time, support and valuable input over the years; thanks to Dr. Richard Zeebe for all of his insight, guidance and support over the years while I have been working on my thesis research.

I would like to thank Dr. Brian Powell and Dr. Tobias Friedrich for allowing me to access and use ROMS products and for their valuable input regarding the comparisons between the ROMS and hybrid models. I am immensely grateful to Dr. Eric Firing for his assistance developing code using the Python programming language. I'm thankful for all of the office administrative support from Kristin Momohara and other office staff members at the University of Hawai‘i at Mānoa, School of Ocean and Earth Science and Technology. Thank you to all of the cruise planners, captains, crew members and scientists responsible for organizing each of the cruises and for collecting and analyzing the incredible 30-year Hawai‘i Ocean Time-series dataset; this thesis research would not have been possible without them. I would also like to thank Dr. Hannah Barkley, Dr. Melissa Meléndez and Amy Markel for their assistance with dataset access; thanks again to Dr. Melissa Meléndez for your helpful feedback in preparation for my defense. I would like to thank Lucie Knor for her time and assistance providing technical support and feedback during this research.

I am thankful for the support from my friends and family (special thanks to my mom, Bonner Egan, who has always encouraged me and who has been a tremendous support over the years). I would also like to give special thanks to my husband, Josh Jackson, for his understanding, for always believing in me and for being there for me when I needed it the most.

ABSTRACT

Ocean acidification (OA) is a growing global environmental concern with impacts affecting regions all over the world, including remote areas such as Hawai‘i. OA is gaining worldwide attention due to environmental impacts including the detrimental effects of OA on coral reefs. Increased anthropogenic release of CO_2 into the atmosphere will result in increased absorption by the world oceans. There is a general lack of information regarding small-scale spatiotemporal variations in surface ocean carbon parameters, however satellites and other remote sensing platforms are becoming increasingly utilized for Earth system observations and can be used to help evaluate OA patterns around Hawai‘i. With the use of empirical algorithms, remote measurements of sea surface temperature (SST) and sea surface salinity (SSS) can be used to assess OA patterns in coastal and open-ocean waters around the state. For the purposes of this study, in situ data collected from mooring buoys and ship studies are used to develop empirical algorithms that relate satellite observations to OA conditions for the Hawaiian Islands region (HIR).

TABLE OF CONTENTS

LIST OF TABLES

LIST OF FIGURES

CHAPTER 1. INTRODUCTION

Ocean acidification (OA) occurs when atmospheric carbon dioxide enters the ocean and reacts with water molecules to form carbonic acid and its dissociation products. An increase in fossil fuel emissions produce elevated concentrations of carbon dioxide (CO_2) that enter the Earth's atmosphere, which are then absorbed by the world oceans through direct chemical exchange (Heinze et al., 2015). The ocean acts as a natural carbon sink and ~90% of the total dissolved inorganic carbon in seawater is stored as bicarbonate (HCO_3^-), ~10% is stored as carbonate (CO_3^{2-}) and < 1% is stored as aqueous CO_2 (Barker & Ridgwell, 2012). A study from 1994-2007 estimated the average uptake rate of global anthropogenic carbon to be 2.5 ± 0.3 Petagrams of Carbon per year (Pg C yr^{-1}); the global inventory of anthropogenic carbon was estimated to reach 159 ± 20 Pg C by 2010 (Gruber et al., 2019).

When atmospheric CO_2 enters the ocean surface, a series of reactions occur. The first reaction in this process occurs when CO_2 reacts with water to form carbonic acid (H_2CO_3):

$$CO_2 + H_2O \rightarrow H_2CO_3 \qquad \textbf{(1)}$$

Next, carbonic acid dissociates into HCO_3^- through the loss of a hydrogen atom:

$$H_2CO_3 \rightarrow H^+ + HCO_3^- \qquad \textbf{(2)}$$

Most, but not all, of the hydrogen ions from the above reaction will bind to a carbonate ion (CO_3^{2-}) to form bicarbonate:

$$H^+ + CO_3^{2-} \rightarrow HCO_3^- \qquad \textbf{(3)}$$

As more free hydrogen ions become available, the pH of seawater decreases. Concentration ratios of particular carbon species can be determined by the pH level. **FIGURE 1** below

illustrates this concept using a Bjerrum plot. As pH decreases, carbonate ion concentrations decrease dramatically while bicarbonate ion concentrations increase.

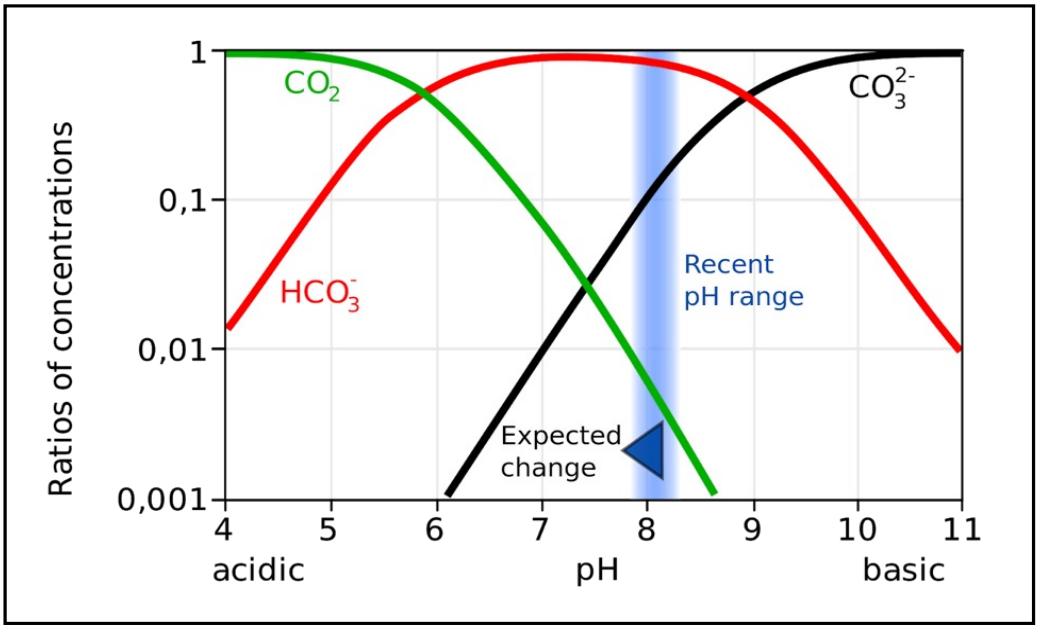

FIGURE 1

A Bjerrum plot displaying concentrations of carbon dioxide, bicarbonate, and carbonate ions at varying pH levels. As hydrogen ions increase in seawater, pH decreases resulting in lower concentrations of carbonate ions. (https://en.wikipedia.org/wiki/Bjerrum_plot).

As OA reduces the carbonate ion concentrations, many marine organisms that form their shells from calcium carbonate ($CaCO_3$) minerals will become increasingly vulnerable to OA. Two commonly found mineral forms of biologically produced $CaCO_3$ are aragonite and calcite. Aragonite is more soluble than calcite, meaning that it is easier for the mineral to dissolve in the surrounding environment, or conversely more difficult to form with rising OA (Haigh et al., 2015).

The aragonite saturation state value, represented by the symbol Ω_{Ar}, will indicate whether calcium carbonate is saturation ($\Omega_{Ar} = 1$), supersaturated ($\Omega_{Ar} > 1$) or undersaturated ($\Omega_{Ar} < 1$) in certain areas. As Ω_{Ar} increases, precipitation of $CaCO_3$ becomes thermodynamically more

favorable, which drives calcification rates for marine organisms (e.g., corals) (Cyronak et al., 2016).

Alternatively, when Ω_{Ar} decreases below a value of 1, $CaCO_3$ dissolution occurs. As a result, organisms will need to dedicate more energy into building their shells when the rate of dissolution exceeds the rate of accretion (Haigh et al., 2015). Ω_{Ar} is commonly used to track OA because of the relationship between carbonate ion concentrations, the primary driver of Ω_{Ar} variations, and the stability of this important mineral produced by marine organisms (Dunne et al., 2013).

The precipitation or dissolution of carbonate minerals, such as aragonite, can be expressed as:

$$CaCO_3\ (s) \rightarrow CO_3^{2-} + Ca^{2+} \qquad \textbf{(4)}$$

Equation (5) below can be used to determine the extent of aragonite saturation in seawater:

$$\Omega_{Ar} = [CO_3^{2-}][Ca^{2+}]/K_{sp} \qquad \textbf{(5)}$$

In **Equation (5)**, K_{sp} represents the equilibrium solubility product of aragonite at a specific temperature, salinity and pressure.

Organismal responses to increased OA will vary across many species (i.e., decreased shell sizes, reproductive changes, etc.), with some tolerance to changes greater than others (Kroeker et al., 2013). For instance, as the ocean acidifies, molluscs such as oysters and scallops may find it more difficult to build and maintain their shells. As a result, fisheries that heavily depend on molluscs would likely experience negative impacts. Coral reef ecosystems, a prominent feature of the Hawai‘i coastline, are also susceptible to OA and other effects resulting from climate change. Loss of coral reef ecosystems could have profound effects on marine biodiversity by impacting organisms that feed and reproduce on the reefs (Doney et al., 2020). It has been found that as sea surface temperatures increase, a phenomenon known as “coral bleaching” can occur,

which impairs the ability of corals to grow their skeletons. While it has been challenging to directly link changes in net coral accretion rates to OA specifically, results from an alkalinity (A_T) enrichment study found that when seawater carbonate ions are increased to preindustrial levels, net community calcification increases; results from this study suggest a direct correlation between OA and net community calcification (Doney et al., 2020).

SST, SSS and Ω_{Ar} are among three of the most important factors controlling the geographic distribution of coral reefs in shallow waters. Habitat changes caused by global warming, OA and other environmental factors can negatively impact shallow-water corals. Annual and spatially averaged tolerance limits have been established using a diagnostic ReefHab model (Kleypas, 1995). Responses of coral reefs to changing environmental conditions is variable and Ω_{Ar} tolerance limits vary depending upon environmental factors and based on species-level adaptability; even within the same species, factors such as minimum light tolerance can differ based on morphological differences. Field investigations suggest a natural Ω_{Ar} limit of 2.9; however, in other areas such as the Great Barrier Reef, findings suggest a lower threshold value of 2.82 (Guan et al., 2015). An earlier study by Kleypas et al., 1999 indicates a minimum Ω_{Ar} tolerance of 3.28.

Due to the prevalence of marine life, widespread coral reef ecosystems, and a reliance on fishing in Hawai‘i, an increased intensity of effects resulting from OA on the surrounding local environment and population is anticipated. Seafood is a major dietary component for many residents and vacationers in Hawai‘i. Including noncommercial catch, 51% of the total seafood available for consumption is locally sources (Loke et al., 2015). Evidence suggests that elevated CO_2 concentrations affect the physiology and survival of many marine organisms, including fish. A number of fish species are sensitive to the effects of OA; changes in larval physiology, growth and survival rates have been observed and vary on a species level (Scholey et al., 2012). Over the past decade, decreasing trends in ocean pH, another common parameter for monitoring OA, are of greater global concern, which has gained widespread attention from scientists and politicians. Carbon dioxide, upwelling and nutrient pollution all contribute to decreases in ocean pH. Long-term time series analyses using Hawai‘i Ocean Time-series (HOT) program data indicate a

decreasing trend in ocean pH and carbonate ion concentrations (**FIGURE 2**) in the North Pacific Ocean since 1989. Since the beginning of the industrial revolution, ocean pH has dropped by ~0.1. This value alone may not seem dramatic but is equivalent to a 26% increase in ocean acidity (Pidcock, 2015).

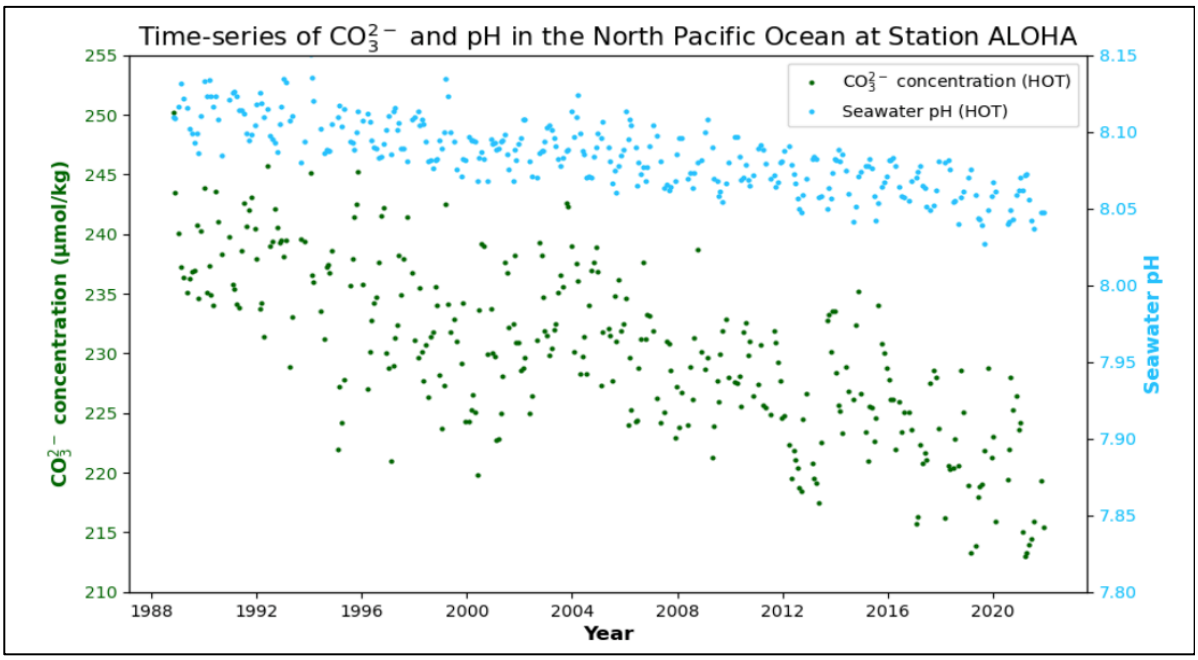

FIGURE 2

Time-series of CO_3^{2-} and pH at the ocean surface (< 50 m) in the North Pacific Ocean at Station ALOHA from 1989-2021. Trends are based on in situ observations made available by the Hawai‘i Ocean Time-series (HOT) program (https://hahana.soest.hawaii.edu/hot/hotco2/hotco2.html).

OA is not spatially constant or homogeneously distributed. Carbonate system monitoring has been primarily conducted from ship- and field-based studies. These approaches are limited in space and time and provide sparse measurements (Land et al., 2019); in order to observe more localized effects of OA, new studies focusing on remote observations of carbonate system parameters have been developed.

Fluctuating relationships between Ω_{Ar} and other variables across ocean regimes establishes a need for the development of regional models. The use of satellite algorithms for data optimization, coverage and resolution is a relatively new development. Use of satellite measurements and applied algorithms are beneficial because they overcome spatial limitations and undersampling biases that can be challenging when working with in situ measurements. The developed algorithms can be used to calculate Ω_{Ar} with near real-time availability and with minimal spatial extrapolation. The algorithms were developed in accordance with methods established in the literature from similar studies in other tropical regions (e.g., Gledhill et al., 2008).

Over the past few decades, thermal cameras and microwave sensing technologies have been used to measure ocean sea surface temperature (SST) and sea surface salinity (SSS) from space. Although satellites cannot directly measure OA, the measurements collected can be exploited for more rapid and expansive estimates of certain OA proxies (Land et al., 2015). Utilizing satellite-based measurements to create geospatial maps of Ω_{Ar} and other OA related parameters across the HIR (including remote areas surrounding the main Hawaiian Islands (MHI) will provide widespread and near real-time information, which has the potential to reduce uncertainties with respect to the local carbon budget (Lohrenz et al., 2018). This approach can provide new information spanning large geographic domains, allowing scientists to evaluate OA patterns and variations on regional and global scales. Knowledge obtained will be critical for resource managers and local marine industries.

Incorporation of satellite measurements provides widespread coverage and near real-time information. Empirical algorithms derived from hydrographic measurements such as SST, SSS and ΔpCO_2 will allow for the development of regional maps that display surface ocean variability of Ω_{Ar} across the HIR. Geospatial mapping of near real-time OA approximations for the surface ocean across the HIR can be used to define and evaluate local OA parameters and to make assessments about surrounding oceanic and environmental health.

This thesis examines the following hypotheses with respect to the spatial and temporal patterns of OA in the HIR,

1. The calcification on coral reefs can change the linearity of the slope of the sea surface salinity (SSS) vs. total alkalinity (A_T).
2. Sea surface Ω_{Ar} values will be higher to the west in the Hawaiian Islands Region (HIR) based on the movement of surface currents.
3. Surface ocean Ω_{Ar} values will be primarily driven by changes in sea surface temperature (SST).
4. There will be a long-term decrease in surface ocean Ω_{Ar} values which will cross a "coral threshold", where the corals can no longer sustain themselves, within the next 30 years.

CHAPTER 2. METHODS AND APPROACH

The study domain encompasses waters from 150.1 to 164°W and 18-24°N, here-after referred to as the HIR. The HIR includes islands such as Niʻihau, Oʻahu, Molokaʻi, Kauaʻi, Lanaʻi, Kahoʻolawe, Maui and the Island of Hawaiʻi (or otherwise commonly referred to as the Big Island). Ω_{Ar} values for the HIR were calculated from regionally- and empirically-derived algorithms developed from ordinary least squares (OLS) regression techniques. In order to estimate inorganic carbon variables from hydrographic measurements, the initial algorithms were developed from in situ measurements of SST, SSS, A_T, pCO_2, and in some cases, dissolved inorganic carbon (C_T). Some of these measurements are frequently observed using autonomous platforms and datasets are widely available.

A_T is a quasi-conservative carbonate system parameter and can be estimated independently from SSS and SST using site-specific algorithms. SSS, however, is the largest driver of seawater ionic composition and is strongly related to A_T (Land et al., 2019). It can be more challenging to estimate A_T in coastal regions due to biological influence and/or from changes in A_T due to riverine discharge, groundwater input and/or upwelling. Jones et al. (2016) found that incorporating SST into algorithms used for A_T calculations will increase regional A_T predictability and may serve as a proxy for A_T changes that may be caused by upwelling processes. Algorithms were developed for A_T and seawater pCO2 ($pCO_{2,\,sw}$); next, values were substituted into a Python-based package called PyCO2SYS (Humphreys et al., 2022) in order to calculate Ω_{Ar}.

Station ALOHA (A Long-term Oligotrophic Habitat Assessment, a deep-water station located approximately 100 km north of Oʻahu at 22.75°N, 158°W) is one of the in situ data collection sites used to develop the open ocean A_T algorithm. Discrete measurements of carbonate system parameters were obtained from CTD casts and bottle samples collected from Station ALOHA during the Hawaiʻi Ocean Time-series (HOT) research cruises from January 1989 to December 2020 (all HOT data were obtained via the Hawaiʻi Ocean Time-series HOT-DOGS application, https://hahana.soest.hawaii.edu/hot/hot-dogs/interface.html. Accessed in December 2022).

Shipboard measurements collected during the Hawai‘i Ocean Time-series cruises, the Global Ocean Data Analysis Project or GLODAP (Olsen et al., 2016) cruise numbers 306, 1043 and 1044 from March 2006 and May 2015, and Surface Ocean CO_2 ATlas or SOCAT (Bakker et al., 2016) cruises were used to develop the open ocean algorithms. Data collected from local mooring buoys surrounding O‘ahu from 2009-2019 and from the 2019 National Coral Reef Monitoring Program or NCRMP (Barkley et al., 2021) were used to generate the coastal algorithms. **TABLE 1** summarizes the data sources and parameters used for generating each of the open ocean algorithms. **TABLE 2** summarizes the data sources and parameters used for generating each of the coastal algorithms.

TABLE 1. DATA SOURCES AND INFORMATION USED FOR GENERATING OPEN OCEAN ALGORITHMS

Shipboard measurements collected during multiple research cruises and used as inputs for the generation of open ocean algorithms (SSS = sea surface salinity, SST = sea surface temperature, D = depth, A_T = total alkalinity, ΔpCO_2 = pCO_2 (seawater) – pCO_2 (air)).

Data source	Collection method(s)	Parameters	Location	Dates	Algorithm
Hawai‘i Ocean Time-series	Bottle samples; CTD	A_T, D, SSS, SST	Station ALOHA (22.75˚N, 158˚W)	01/1989-12/2020	A_T
Global Ocean Data Analysis Project (GLODAP – v2.2022) cruises	Bottle samples; CTD	A_T, D, SSS, SST	Variable	03/2006-05/2010	A_T
Surface Ocean CO_2 ATlas (SOCAT) cruises	Bottle samples; CTD	ΔpCO_2, D, SSS, SST	Variable	06/2008-05/2017	ΔpCO_2

TABLE 2. DATA SOURCES AND INFORMATION USED FOR GENERATING COASTAL ALGORITHMS

Sources of measurements used as inputs for the generation of coastal algorithms. (SSS = sea surface salinity, SST = sea surface temperature, D = depth, A_T = total alkalinity, ΔpCO_2 = pCO_2 (seawater) – pCO_2 (air)).

Data source	Collection method(s)	Parameters	Location	Dates	Algorithm
National Coral Reef Monitoring Program (NCRMP) cruises	Bottles samples; CTD	A_T, D, SSS, SST	Variable	04/2019-09/2019	A_T
Ala Wai (MAPCO2 mooring)	Bottle samples	A_T, D, SSS, SST	21.28˚N, 157.85˚W	02/2014-08/2019	A_T
Kilo Nalu (MAPCO2 mooring)	Bottle samples	A_T, D, SSS, SST	21.29˚N, 157.87˚W	01/2015-12/2019	A_T
Kāneʻohe (MAPCO2 mooring)	Bottle samples	A_T, D, SSS, SST	21.48˚N, 157.78˚W	02/2016-05/2016	A_T
Surface Ocean CO_2 ATlas (SOCAT) cruises	Autonomous, bottle samples, CTD	ΔpCO_2, D, SSS, SST	Variable	12/2005-05/2013	ΔpCO_2

2.1 ORDINARY LEAST SQUARES (OLS) REGRESSION MODEL

An OLS regression model was used to relate A_T values within the study domain to SSS and SST values. Relationships between carbonate system parameters and SSS and SST are primarily influenced by thermodynamics (Land et al., 2019); changes in SST and SSS as a result of dilution, evaporation, precipitation and ice melting/freezing can influence the number of ions present in seawater. SST does not have a direct effect on A_T but does share a correlation; as SST decreases, A_T increases. SST values can be used to indicate where the seawater has come from and lower SST values can be used to identify upwelling processes, bringing colder water with higher A_T values to the sea surface.

SSS and A_T share a positive linear relationship with one another in the open ocean. In coastal settings, relationships between A_T and SSS are strongly affected by chemical processes such as weathering, nutrient runoff, pollution, calcification and dissolution (Land et al., 2019) – more specifically, the dissolution of calcium carbonate ($CaCO_3$) can potentially alter and decouple the linear relationship between A_T and SSS.

Biological constraints on the marine carbonate system include, but are not limited to, processes such as primary production, calcification, respiration and remineralization (Land et al., 2019). Freshwater flux, changes in SST, biological activity, nutrient cycling, upwelling and other biological and/or physical processes can affect A_T. In order to account for these constraints on A_T, they are corrected for using site-specific algorithms based on geographic location and proximity to land.

2.2 ESTABLISHING AN OPEN OCEAN ALGORITHM FOR A_T

In order to develop an empirical algorithm for calculations of A_T for the open ocean, in situ measurements of SST, SSS, A_T and D were obtained from datasets collected during HOT and Global Ocean Data Analysis Project (GLODAP) oceanographic research cruises; each of these datasets represents the open ocean regime.

32 measurements collected from GLODAP cruises 306, 1043 and 1044 from March 2006 and May 2015 were combined with 595 HOT cruise measurements in order to develop an open ocean algorithm for A_T. **FIGURE 3** below illustrates the geographic locations for each of the data collection sites.

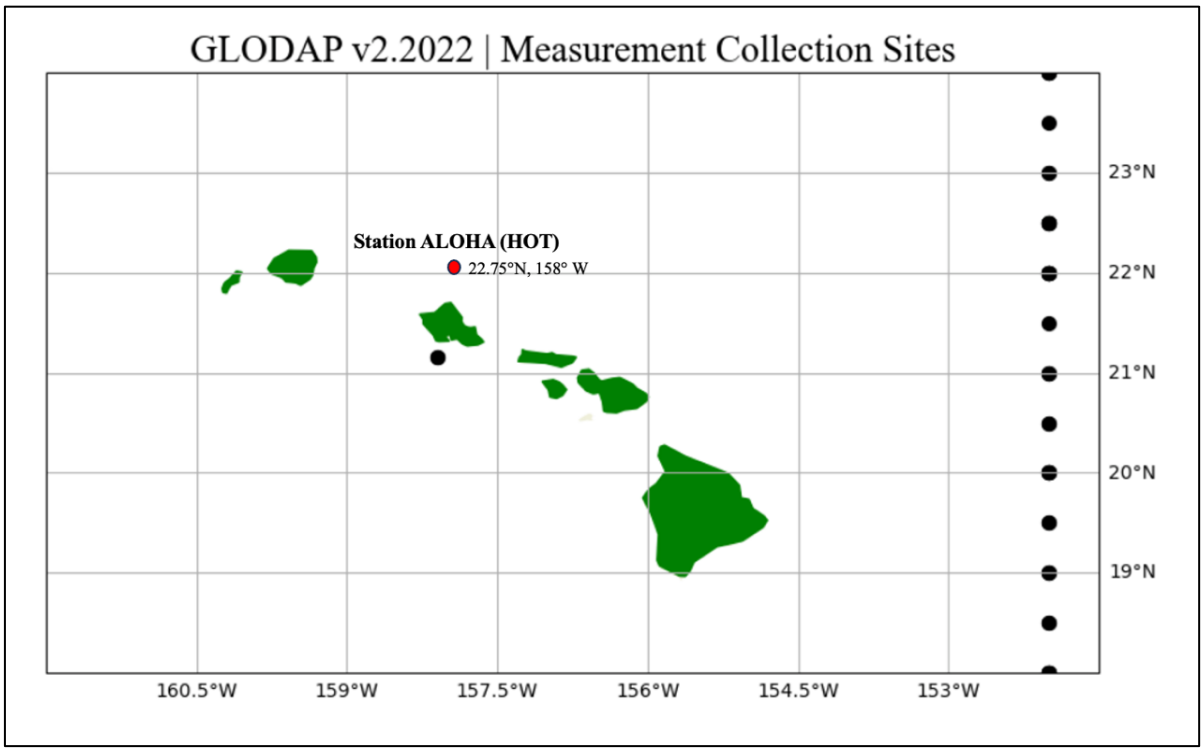

FIGURE 3

The location of water samples collected (red circle) during the Hawai‘i Ocean Time-series cruises at Station ALOHA (HOT). The location of water samples collected during GLODAP

Quality flag values of 2 (good values) were accepted for A_T and SSS measurements from the GLODAP dataset; methods for QA/QC for all HOT data were previously applied. Depth (D) was constrained to the upper 30 meters for all open ocean SSS and SST measurements collected using CTD and Niskin bottles. The GLODAP and HOT datasets were combined into a single dataset prior to further analyses. After an initial OLS regression was determined, a few outliers

greater than 2σ from the regression line were removed and a final OLS regression was determined.

FIGURE 4 below contains values from the combined HOT and GLODAP datasets and illustrates the linearity between SSS and A_T for the open ocean.

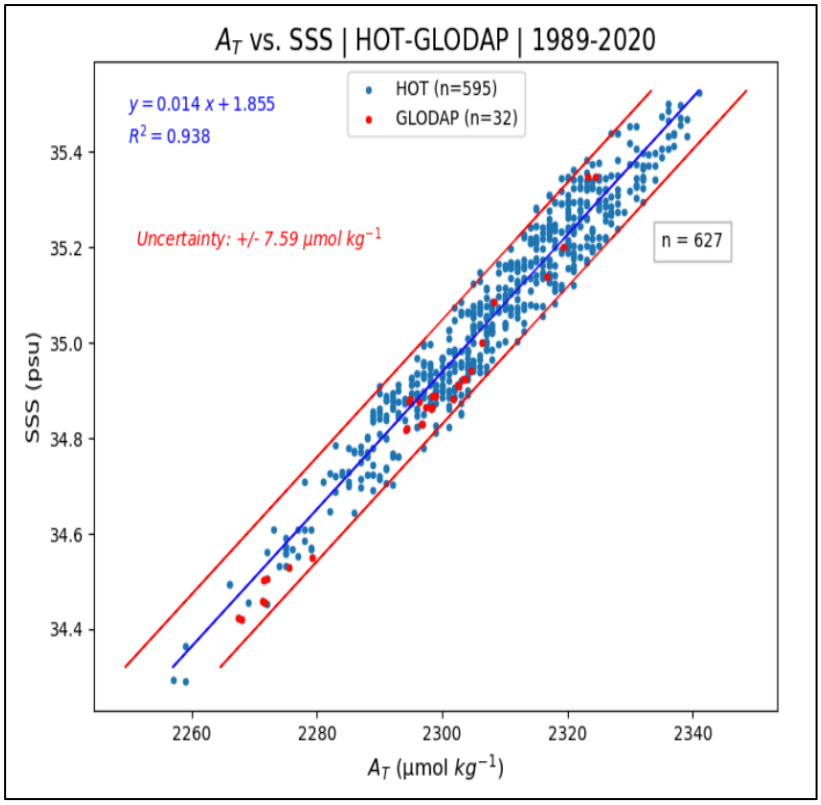

FIGURE 4

A representation of the linear relationship between SSS and A_T from the HOT and GLODAP datasets for the open ocean; $R^2 = 0.938$. HOT values (n = 595) are displayed as blue dots and GLODAP (n = 32) values are displayed as red dots.

An open ocean algorithm for A_T was established using SSS and SST as independent inputs; the R^2 value of the fit is 0.938, indicating that about 93.8% of the variance in A_T values can be

explained by the OLS regression model using SSS and SST. **Figure 5** displays the OLS regression model results used to generate the open ocean algorithm for A_T.

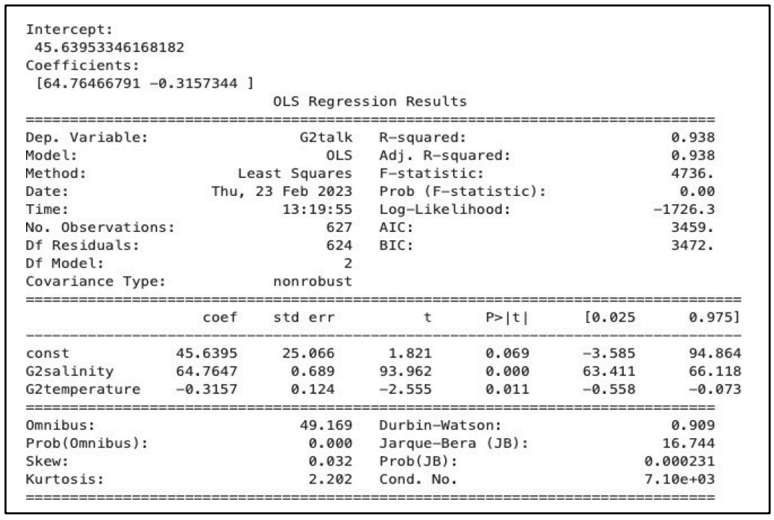

```
Intercept:
 45.63953346168182
Coefficients:
 [64.76466791 -0.3157344 ]
                            OLS Regression Results
==============================================================================
Dep. Variable:                 G2talk   R-squared:                       0.938
Model:                            OLS   Adj. R-squared:                  0.938
Method:                 Least Squares   F-statistic:                     4736.
Date:                Thu, 23 Feb 2023   Prob (F-statistic):               0.00
Time:                        13:19:55   Log-Likelihood:                -1726.3
No. Observations:                 627   AIC:                             3459.
Df Residuals:                     624   BIC:                             3472.
Df Model:                           2
Covariance Type:            nonrobust
==============================================================================
                 coef    std err          t      P>|t|      [0.025      0.975]
------------------------------------------------------------------------------
const         45.6395     25.066      1.821      0.069      -3.585      94.864
G2salinity    64.7647      0.689     93.962      0.000      63.411      66.118
G2temperature -0.3157      0.124     -2.555      0.011      -0.558      -0.073
==============================================================================
Omnibus:                       49.169   Durbin-Watson:                   0.909
Prob(Omnibus):                  0.000   Jarque-Bera (JB):               16.744
Skew:                           0.032   Prob(JB):                     0.000231
Kurtosis:                       2.202   Cond. No.                     7.10e+03
==============================================================================
```

FIGURE 5

Results from an OLS regression model used to generate an open ocean algorithm for A_T.

Equation (6) below is the open ocean algorithm generated for calculating A_T along with the coefficient of determination (R^2) value:

$$A_T = 64.8(SSS) - 0.3(SST) + 45.6;\ R^2=0.938 \qquad \textbf{(6)}$$

SST was included in the open ocean algorithm for A_T calculations in an effort to enhance the predictability of open ocean A_T values. While SST does not have a direct effect on A_T values, there is a correlation. As SST decreases, A_T values increase (Millero et al., 1998); for that reason, SST can be used as a proxy for changes in A_T due to upwelling (Lee et al., 2006). The inclusion of SST in the OLS regression model slightly reduces the standard error of the calculation.

2.3 EXAMINING COASTAL A_T VS. SSS RELATIONSHIPS

Coastal A_T vs. SSS relationships were examined using data collected from the Kilo Nalu (n = 36), Kāneʻohe (n = 25) and Ala Wai (n = 36) mooring buoys surrounding Oʻahu and from the NCRMP measurements collected along the coastlines of the MHI. **FIGURE 6** below illustrates the NCRMP coastal measurement collection sites (n = 309) for the MHI.

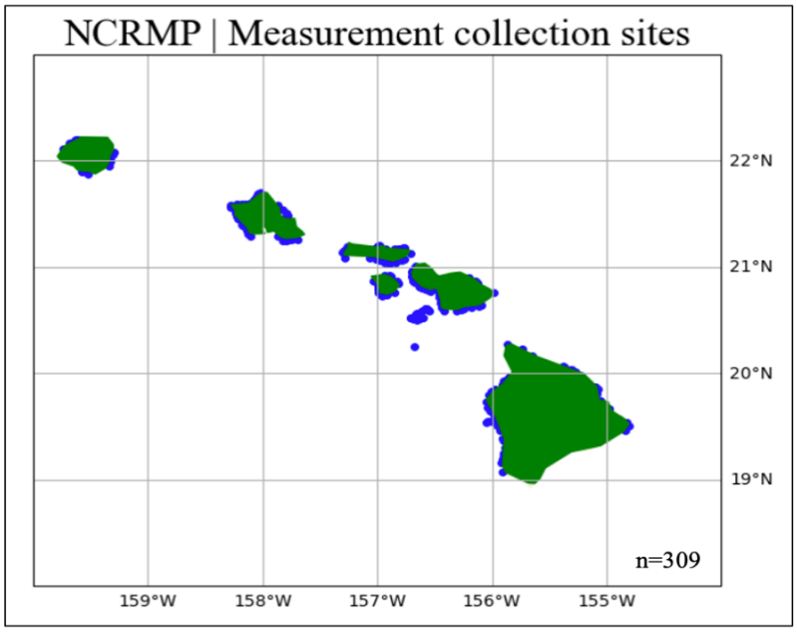

FIGURE 6

NCRMP coastal measurement collection sites (blue) for the MHI (n = 309).

To explore how coastal A_T vs. SSS relationships may differ from open ocean relationships, an A_T vs. SSS plot was constructed to collectively compare all coastal values with the open ocean trend. **FIGURE 7** below displays A_T vs. SSS relationships for all coastal (blue) and open ocean (red) values.

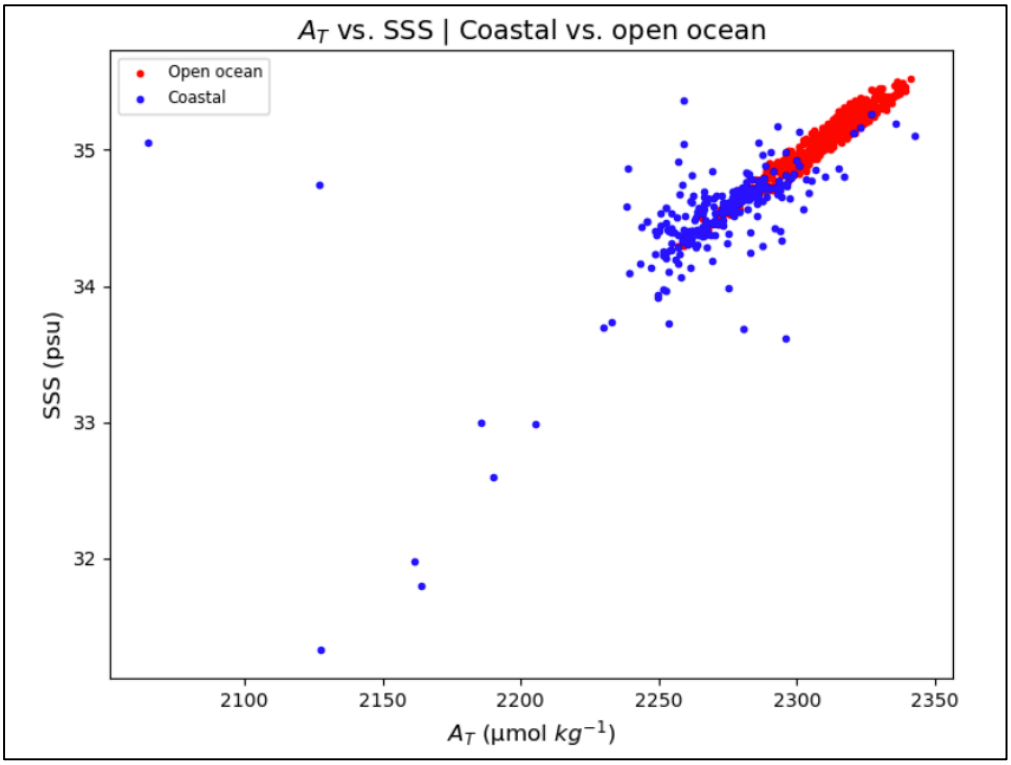

FIGURE 7

A_T vs. SSS plot comparing open ocean (red) with coastal (blue) values.

Although some overlap exists between the coastal and open ocean values, A_T vs. SSS relationships appear to be more variable for coastal waters than they are for the open ocean; this variability could be the result of enhanced biological productivity, introduction of freshwater from point sources, nutrient runoff from land, etc. It was determined that all of the coastal measurements collected from areas surrounding the Big Island and Ni‘ihau overlapped with open ocean values; therefore, the open ocean A_T algorithm was assigned to coastal waters surrounding these islands.

A_T vs. SSS plots for the remaining coastal waters did appear to have different slopes relative to the open ocean trendline (**FIGURE 8**).

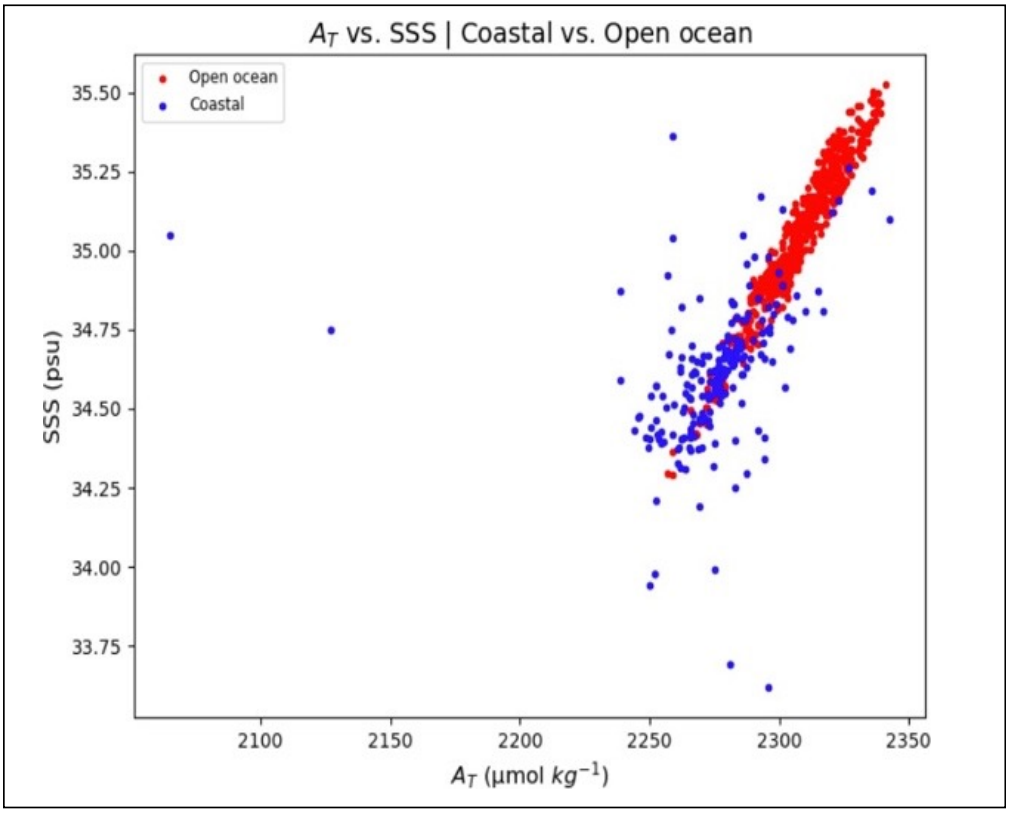

FIGURE 8

A_T vs. SSS plot comparing open ocean (red) with coastal (blue) values. Values collected from coastal waters surrounding the Big Island and Ni‘ihau are excluded.

To further investigate the variability observed with respect to coastal A_T vs. SSS relationships, the spatial distribution of coastal measurements for O‘ahu, Moloka‘i, Lanai, Kaho‘olawe and Maui were considered separately. Coastal measurements often appeared in clusters and were surrounded by gaps (where measurements were unavailable). For this reason, clusters of values were frequently grouped together for comparison purposes.

The greatest difference between A_T vs. SSS relationships occurs for measurements collected along the northeastern and southeastern shorelines of O‘ahu (illustrated in **FIGURE 9** below). Values for all other islands (including coastal measurements for coastal waters surrounding the northwest and southwest portions of O‘ahu) are shown in blue.

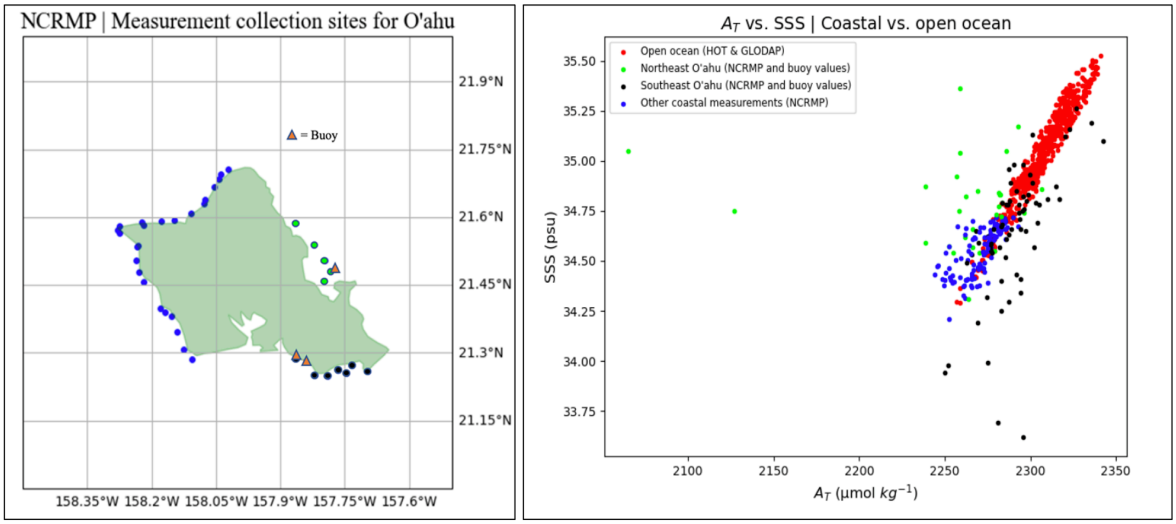

FIGURE 9

NCRMP and buoy measurement collection sites for waters surrounding O‘ahu (left). All coastal values were compared with open ocean values (right). Measurements collected for southeast O‘ahu are displayed in black and measurements collected for northeast O‘ahu are displayed in green. Coastal measurements for each of the other islands (including northwest and southwest O‘ahu) are displayed in blue.

Since A_T vs. SSS relationships along the northeastern and southeastern waters of O‘ahu appear to express the greatest levels of variability when compared with all other coastal values, these two areas are considered to be distinct and as such, required the construction of separate algorithms for A_T calculations.

After identifying the areas with the greatest levels of variability, all of the remaining coastal measurements (blue) were then compared. **FIGURE 10** below illustrates the remaining coastal measurements that were considered in order to determine if additional coastal A_T algorithms were needed.

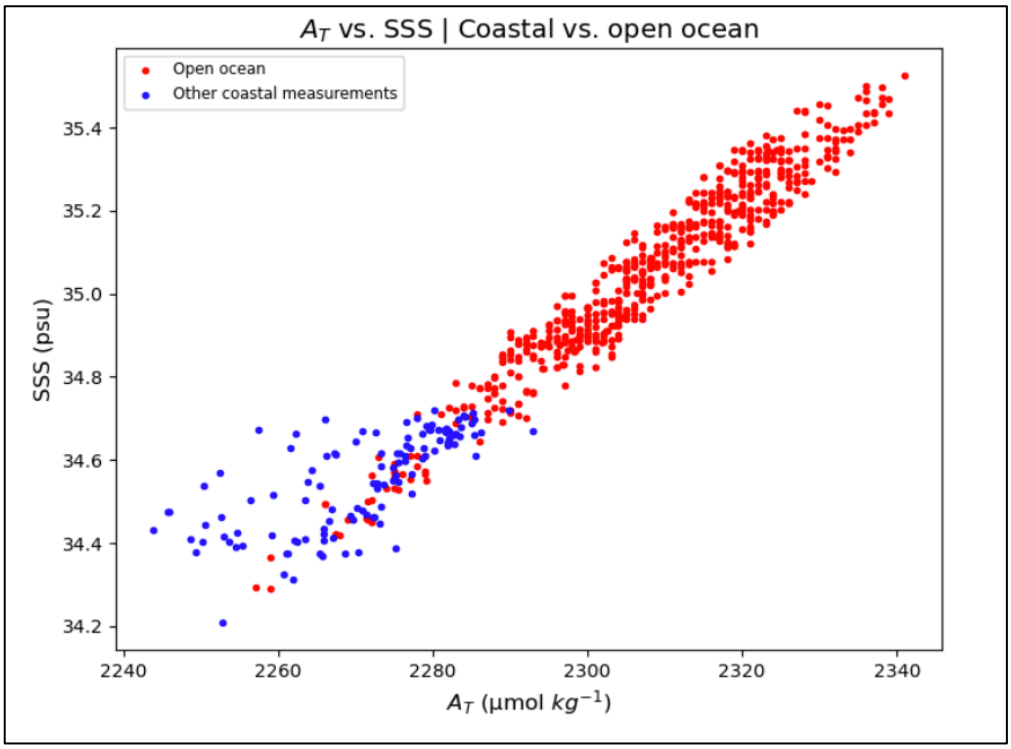

FIGURE 10

Remaining coastal measurements that were considered in order to determine if additional A_T algorithms were needed.

All of the remaining coastal measurements were organized based on geographic proximity; in other words, measurements that occurred in clusters were grouped together for all remaining coastal areas across the MHI. A_T vs SSS relationships for each group were then compared against the open ocean trendline; groups with values occurring within the open ocean value range (cyan) were assigned to the open ocean algorithm for A_T calculations; groups with values extending beyond the range of open ocean values were further classified based on A_T and slope value differences; groups with similar slope values were combined to form a subgroup. Ultimately, a total of two coastal subgroups (in addition to the subgroups established for southeast and northeast O‘ahu) were established using this method and are displayed in **FIGURE 11** below. A single value (blue) occurring outside of the range of open ocean values was most closely aligned with values for southeast O‘ahu (right) and was assigned to the southeast O‘ahu subgroup.

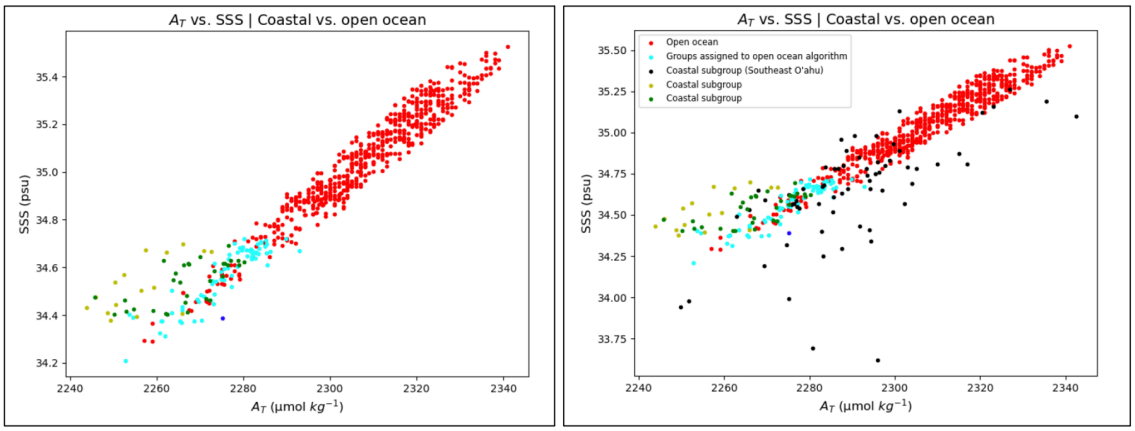

FIGURE 11

A_T vs. SSS relationships for each subgroup. Subgroups containing values occurring within the range of open ocean values (cyan) were assigned to the open ocean algorithm for A_T calculations. A single value (blue) occurring outside of the range of open ocean values was most closely aligned with values for southeast O‘ahu (black) and was assigned to the southeast O‘ahu subgroup (displayed on the right).

2.4 ESTABLISHING COASTAL ALGORITHMS FOR A_T

A total of four coastal subgroups were established using the grouping methods described in **2.3 EXAMINING COASTAL A_T VS. SSS RELATIONSHIPS**. After each of the subgroups were established, outlier values > 2σ from the mean distribution were removed before executing the final OLS regressions for each subgroup in order to generate four coastal A_T algorithms.

Subgroup #1:

$$A_T = 20.0(SSS) - 8.0(SST) + 1{,}786.7;\ R^2 = 0.147 \qquad \textbf{(7)}$$

Subgroup #2:

$$A_T = 48.6(SSS) - 0.3(SST) + 598.0;\ R^2 = 0.622 \qquad \textbf{(8)}$$

Subgroup #3:

$$A_T = 39.7(SSS) + 3.2(SST) + 801.3;\ R^2 = 0.622 \qquad \textbf{(9)}$$

Subgroup #4:

$$A_T = 50.6(SSS) + 1.1(SST) + 490.5;\ R^2 = 0.481 \qquad \textbf{(10)}$$

The resulting trendlines for each of the four subgroups are displayed in **FIGURE 12** below.

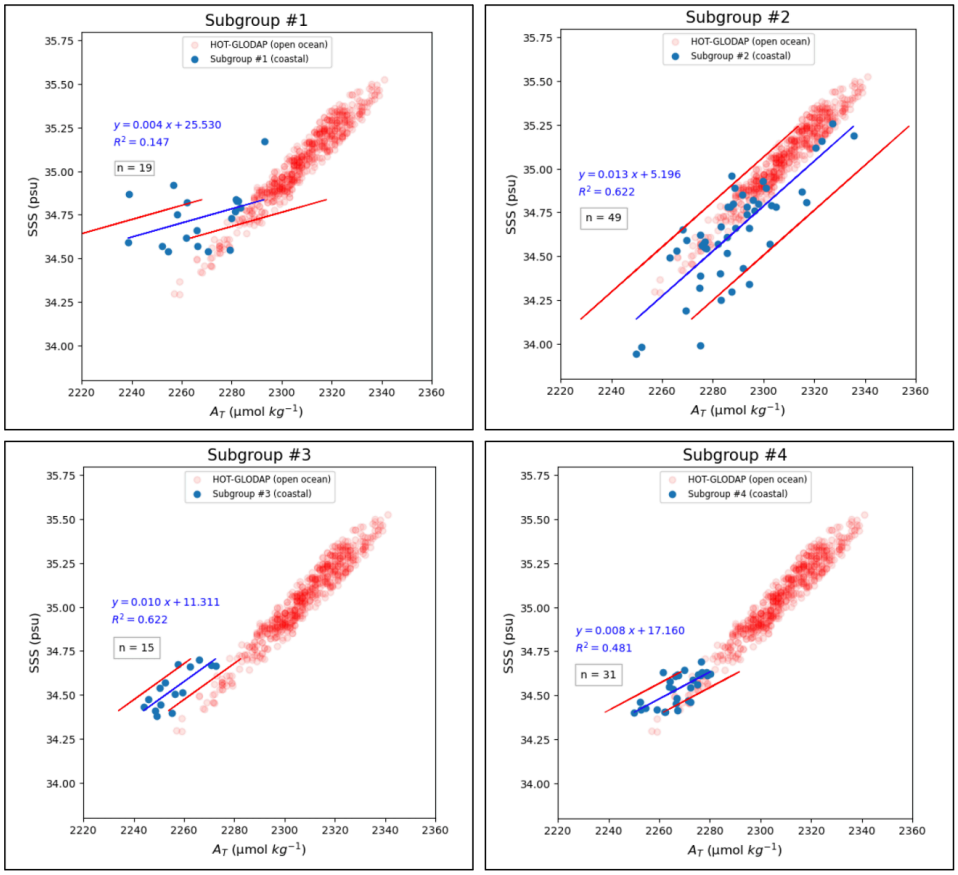

FIGURE 12

Subgroups used for constructing coastal A_T algorithms. Each of the coastal subgroup values (blue) are displayed against the open ocean values (red). Statistical information is included for each group.

2.5 EFFECTS OF CORAL CALCIFICATION ON A_T

Kāneʻohe Bay, the largest sheltered body of water in Hawaiʻi, is a complex estuarine system consisting of patch and fringing reefs and it has been observed that intense calcification rates affect A_T in these areas. Findings indicate that biogeochemically induced changes in A_T were greater than they were for SSS, which modifies the A_T vs. SSS relationship. This study found the largest scatter and change in A_T vs. SSS relationship near Kāneʻohe Bay, which is attributed primarily to the documented intense calcification rates in this area. Although the SSS-A_T correlation for this region was quite low, the OLS fit was the best first approximation of A_T possible at this time.

While Kāneʻohe Bay is uniquely characterized and contains multiple stream inputs (i.e., Kāneʻohe Stream, Kawa Stream, etc.) longer residence times, etc., daily net ecosystem calcification (NEC) was found to be comparable to or higher than NEC at other coral reefs (Schamberger et al., 2011). Another study compared reef and open ocean A_T concentrations at 23 coral reef locations across the globe and considered the ΔA_T value as a direct indication of whether net calcification or dissolution was occurring along the reef (Cyronak et al., 2018). Although the effects of coral reef calcification on A_T are not well quantified for coastal areas within the MHI, coastal A_T values appear to be consistently lower than open ocean values for subgroups #1, #3 and #4 while A_T values for subgroup #2 are more similar to the open ocean. It's been observed that there are fewer corals in the subgroup #2 area (later discussed in further detail). Thus, it appears that there is a correlation between the amount of coral cover in a region and a deviation of the SSS-A_T relationship. This connection between the amount of coral cover and deviation of the SSS-A_T relationship was used to infer which of the existing algorithms would be most appropriate to use in areas that had no available in situ carbon system measurements.

2.6 DATA DEFICIENT ZONES (DDZS)

The measurement gaps that exist in areas located in between measurement clusters across the MHI are referred to as data deficient zones, or DDZs. Across the HIR, there are a total of 8 DDZs. The relationship observed between coral calcification and A_T (Schamberger et al., 2011; Cyronak et al., 2018) was considered while assigning algorithms to each DDZ for A_T calculations. To track the abundance of coral located within each DDZ, maps estimating percent coral cover in Hawai‘i were obtained from the Pacific Islands Ocean Observing System or PacIOOS (Franklin et al., 2013, 2014). A Tier Classification System (TCS) was subsequently developed from these maps in order to assign a tier value to each DDZ based on estimated percentages of coral coverage, then related to one of the previously determined algorithms.

2.7 ESTABLISHING A TIER CLASSIFICATION SYSTEM (TCS)

Tier values of 1, 2 or 3 were assigned based upon the most prevalent percentage of coral coverage observed within each DDZ. **TABLE 3** displays each of the tier values along with the corresponding percentages of coral coverage. Consider a zone with > 50% of coral coverage in certain areas; zones with this level of coverage would assume a tier 3 value if this trend is observed for a majority (> 50%) of the total zone area; however, if most of the DDZ is defined by values within the 11-50% coral coverage range, these areas were assigned to a tier value of 2.

TABLE 3. TIER VALUES WITH CORRESPONDING ESTIMATES OF PERCENT CORAL COVERAGE

Tier values of 1, 2 or 3 were assigned to each DDZ based on percent coral coverage, representing 0-10%, 11-50% and 50-100%, respectively.

Tier value	Percent coral coverage
1	0-10
2	11-50
3	50-100

After assigning tier values to each DDZ, each of the 13 measurement clusters that were used to establish the four coastal subgroups (**FIGURE 12**) were similarly assigned to a tier value. Clusters for subgroups #1, #2 and #4 share identical tier value assignments; subgroup #3 consists of measurement clusters with an equal distribution of tier 2 and tier 3 values. **TABLE 4** below summarizes the tier value assignments for measurement clusters within each coastal subgroup.

TABLE 4. TIER VALUE ASSIGNMENTS FOR SUBGROUPS #1-4 FOR ALL ZONES WITH VALUES THAT DID NOT FOLLOW THE OPEN OCEAN A_T VS. SSS TREND

Information for each coastal subgroup including the island name, cluster number, data source and corresponding tier value.

SUBGROUP #1			
Island	**Cluster**	**Data source**	**Tier value**
O‘ahu	1	Kāne'ohe (discrete)	3
O‘ahu	2	NCRMP	3
SUBGROUP #2			
Island	**Cluster**	**Data source**	**Tier value**
O‘ahu	3	Ala Wai (discrete)	1
O‘ahu	4	Kilo Nalu (discrete)	1
O‘ahu	5	NCRMP	1
SUBGROUP #3			
Island	**Cluster**	**Data source**	**Tier value**
Moloka‘i	6	NCRMP	2
Kaho‘olawe	7	NCRMP	2
Kaho‘olawe	8	NCRMP	3
Lanai	9	NCRMP	3
SUBGROUP #4			
Island	**Cluster**	**Data source**	**Tier value**
Maui	10	NCRMP	2
Maui	11	NCRMP	2
Kaua‘i	12	NCRMP	2
Lanai	13	NCRMP	2

Based on tier value similarities for clusters within each subgroup and based on the average of the percent coral cover estimates, coverage appears to increase sequentially from subgroup #2, #4, #3 and #1. The correlation between tier values for clusters within each subgroup was considered

while assigning A_T algorithms to each DDZ. For example, if a DDZ was assigned to a tier value of 2, then the A_T algorithm assigned for subgroup #4 (consisting of clusters with tier values of 2) was used. For one DDZ containing an approximate 50/50 distribution between tier 2 and tier 3 values, the A_T algorithm assigned to subgroup #3 (with an equal distribution of tier 2 and tier 3 values) was used. DDZs with tier values of 1 (indicating between 0-10% of coral coverage) assumed either the open ocean A_T algorithm or the A_T algorithm established for subgroup #2; if percent coral cover in a DDZ was closer to 0%, then the open ocean A_T algorithm was assigned; alternatively, if a DDZ contained closer to 10% of coral coverage, then the A_T algorithm for subgroup #2 was used. A single exception to this method occurs for a tier 2 DDZ located along the southern perimeter of the Big Island. Since similar patterns of coral coverage span a majority of the coastlines that border the Big Island and since there are no other coastal measurements for the Big Island that diverge from the open ocean trendline, the open ocean A_T algorithm was assigned. There were no DDZs that assumed a tier 3 value assignment.

2.8 GENERATING ΔpCO_2 ALGORITHMS FOR OPEN OCEAN AND COASTAL AREAS

Calculated A_T values and one other carbonate system parameter, either pH, C_T or $pCO_{2,\,sw}$, must be input into PyCO2SYS to calculate Ω_{Ar}. For this study, $pCO_{2,\,sw}$ was the preferred second parameter. Previous studies (e.g., Gledhill et al., 2008) have found a strong relationship between ΔpCO_2 and the CO_2 solubility constant (k_0) which can be calculated from SSS and SST measurements (Weiss, 1974) as shown in **Equation (11)** below.

$$\ln k_0 = A_1 + A_2(100/T) + A_3 \ln(T/100) + S[B_1 + B_2(T/100) + B_3(T/100)^2] \quad \textbf{(11)}$$

SSS and SST measurements from the Surface Ocean CO2 Atlas v2.2022 or SOCAT (Bakker et al., 2016) dataset were substituted into **Equation (11)** for the open ocean and coastal areas. Results produced from a multiple linear regression model containing ΔpCO_2 and k_0 variables were used to derive an equation for ΔpCO_2 as a function of k_0. Bathymetry data was used as a filtering mechanism to determine which SOCAT measurements were collected in coastal waters; bathymetry > 500 m was considered to be representative of the open ocean depths and

bathymetry < 500 m was considered as a coastal area. The same group pairings (subgroups #1-4) and outlier removal procedures that were established for coastal A_T algorithms were also utilized for purposes of developing coastal ΔpCO_2 algorithms. In this case, outlier values > 3σ from the mean trend were removed before generating the final OLS regression model to establish open ocean and ΔpCO_2 algorithms.

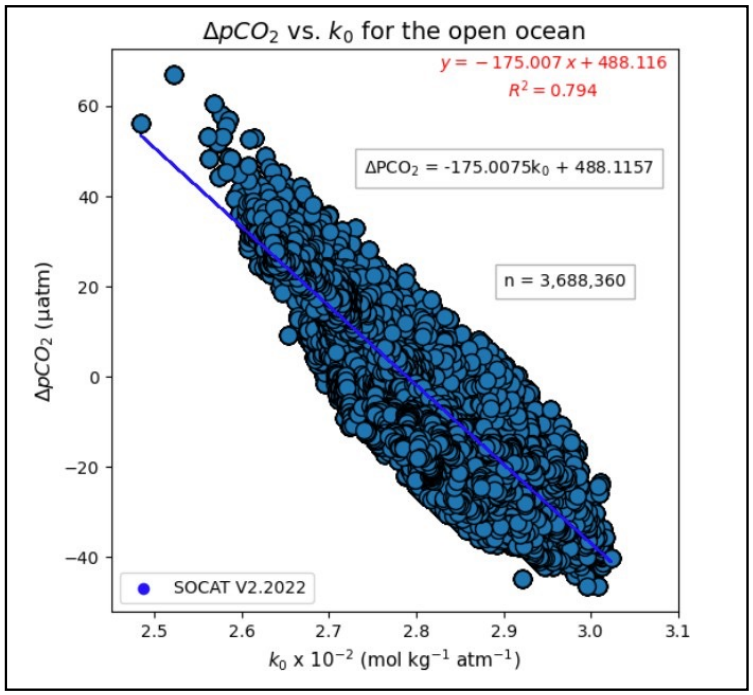

FIGURE 13

Linear fit between ΔpCO_2 and k_0 from the SOCAT v2.2022 dataset for the open ocean; $R^2 = 0.794$. For the open ocean, $\Delta pCO_2 = -175.0k_0 + 488.1$.

FIGURE 14 below displays the results from the linear fits for coastal subgroups #1 and #2. For all measurement clusters within subgroups #3 and #4, there were no corresponding SOCAT values available; NCRMP SSS and SST values for subgroups #3 and #4 were used to calculate k_0; $pCO_{2,\,sw}$ and $pCO_{2,\,atm}$ variables were available from the NCRMP dataset and ΔpCO_2 values were calculated by subtracting $pCO_{2,\,atm}$ from $pCO_{2,\,sw}$ values. Since there were only 15 and 19 NCRMP measurements for subgroups #3 and #4, a subgroup-based ΔpCO_2 algorithm was not

established using these values; ΔpCO_2 vs. k_0 SOCAT values for subgroups #3 and #4 extend beyond the range of open ocean values but are contained within the boundaries for subgroup #2 from the SOCAT dataset. Therefore, the ΔpCO_2 algorithm assigned to subgroup #2 was also assigned to subgroups #3 and #4.

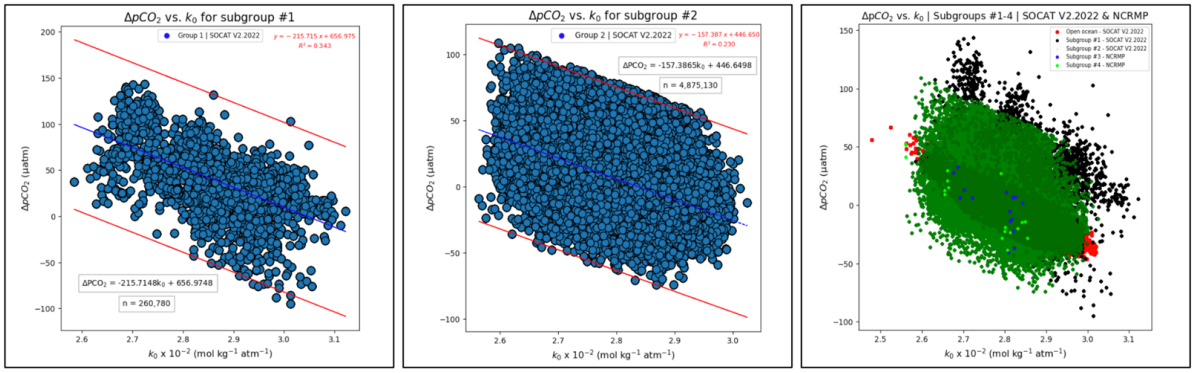

FIGURE 14

Linear fits between ΔpCO_2 and k_0 from the SOCAT v2.2022 dataset for subgroups #1 (left) and #2 (center); for subgroup #1, $R^2 = 0.343$ and $\Delta pCO_2 = -215.7k_0 + 657.0$; for subgroup #2, $R^2 = 0.230$ and $\Delta pCO_2 = 157.4k_0 + 446.6$. For subgroups #3 and #4, SOCAT values were unavailable and NCRMP SSS and SST values were used to calculate k_0. $pCO_{2,\,sw}$ and $pCO_{2,\,atm}$ variables are available from the NCRMP dataset and ΔpCO_2 values were calculated by subtracting $pCO_{2,\,atm}$ from $pCO_{2,\,sw}$ values. A ΔpCO_2 vs. k_0 plot (right) containing SOCAT (subgroups #1 and #2) and NCRMP (subgroups #3 and #4) values was used to determine the appropriate ΔpCO_2 algorithm for subgroups #3 and #4 based on value range similarities.

Each of the subgroup-based coastal ΔpCO_2 algorithms are displayed in **Equations (12) – (13)** below:

Subgroup #1:

$$\Delta pCO_2 = -215.7k_0 + 657.0;\ R^2 = 0.343 \qquad \textbf{(12)}$$

Subgroups #2-#4:

$$\Delta pCO_2 = -157.4k_0 + 446.6;\ R^2 = 0.230 \qquad \textbf{(13)}$$

After ΔpCO_2 algorithms were established for the open ocean and coastal areas, latitude-based $pCO_{2,\,atm}$ values were obtained from the National Oceanic and Atmospheric Administration's Global Monitoring Laboratory (GML) database (https://gml.noaa.gov/ccgg/mbl/data.php); since $pCO_{2,\,atm}$ values provided by GML reflect dry air values (and does not account for water vapor pressure), corrections were applied to account for 100% humidity using the following equation from Weiss and Price, 1980:

$$\ln pH_2O = 24.4543 - 67.4509(100/T) - 4.8489 \ln(T/100) - 0.000544S \quad \textbf{(14)}$$

where pH_2O reflects the vapor pressure in atm, S represents the SSS in ‰ and T represents the SST in Kelvin (K).

Following the calculation of pH_2O, new $pCO_{2,\,atm}$ values were calculated which accounts for water vapor pressure using **Equation (15)** adapted from Dickson et al. (2007):

$$pCO_{2,\,atm\,(wet)} = pCO_{2,\,atm\,(dry)}\,[P_{eq} - pH_2O] \quad \textbf{(15)}$$

where $pCO_{2,\,atm\,(dry)}$ represents monthly atmospheric pCO_2 values derived from the GML database, P_{eq} reflects standard atmospheric pressure, pH_2O is the vapor pressure value calculated from **Equation (14)** and $pCO_{2,\,atm\,(wet)}$ represents the new monthly atmospheric pCO_2 values that have been corrected to account for water vapor pressure.

Latitude was restricted to the HIR and values were averaged for each month from 2015-2020. $pCO_{2,\,sw}$ was calculated by adding ΔpCO_2 and monthly averaged $pCO_{2,\,atm}$ values for all areas within the HIR.

2.9 USE OF PYCO2SYS TO CALCULATE Ω_{AR}

Developed from CO2SYS software, PyCO2SYS is an open-source and Python-based scientific computing package used to carry out marine carbonate system parameter calculations using

automatic differentiation. The components of PyCO2SYS are inherited from CO2SYS-MATLAB v2.0.5 with minimal restructuring to the aesthetic code (Humphreys et al., 2022). Marine carbonate system parameters are solved for following the entry of specific "input" and "output" conditions (i.e., pressure (P), SSS, SST, $pCO_{2,\,sw}$ and A_T) into the PyCO2SYS template code. Ω_{Ar} is one of many output options available.

2.10 FORCING EMPIRICAL ALGORITHMS WITH SATELLITE SSS AND SST MEASUREMENTS

Satellite-based SST products like the Group for High Resolution Sea Surface Temperature (GHRSST) Level 4 Multi-scale Ultra-high Resolution (MUR) Global Foundation Sea Surface Temperature Analysis are made publicly available by the Physical Oceanography Distributed Active Archive Center (PO.DAAC). SST values are available on a global 0.01˚ × 0.01˚ grid.

Satellite-based SSS values were accessed from the Aquarius/SMAP Sea Surface Salinity Optimum Interpolation Analysis product called Multi-Mission Optimally Interpolated Sea Surface Salinity (OISSS) Level 4 V1.0. Monthly repositories are publicly available and accessible via the PO.DAAC THREDDS Data Server through the NASA Jet Propulsion Laboratory (JPL). The OISSS Level 4 V1.0 Monthly product relies on Level-2 orbital swath data from the AQUARIUS/SAC-D mission in order to create a new gridded product. Using optimal interpolation, the OISSS Level 4 V1.0 dataset also utilizes SMAP RSS Level 2 SSS and Soil Moisture and Ocean Salinity (SMOS) Level 2 SSS L2OS data in order to create a grid with a spatial resolution of 0.25˚ and a 4-day temporal resolution (Melnichenko et al., 2021).

2.11 INTERPOLATION OF SATELLITE SSS AND SST VALUES

As shown in **TABLE 5** below, the spatial resolutions of the MUR SST (0.01˚) and OISSS (0.25˚) products differ. Satellite SSS and SST measurements are the baseline parameters for mapping Ω_{Ar} and for this purpose, these products must share a common grid. To achieve this, satellite SST

and SSS data were interpolated to a 0.1˚ × 0.1˚ Cartesian grid using linear interpolation techniques executed by multiple Python scripts.

TABLE 5. SATELLITE-BASED DATA COLLECTION SOURCES AND PARAMETERS

Information regarding satellite sources, data type, parameter, original spatial resolution, temporal resolution and citations are provided. Note: gridded datasets were interpolated to a 0.1˚ × 0.1˚ Cartesian grid.

Satellite sources	Data type	Parameter	Original spatial resolution (˚)	Temporal resolution	Citation
Multi-scale Ultra-high Resolution (MUR) Level 4 V4.1	Grid	SST	0.01 × 0.01	Monthly	JPL MUR MEaSUREs Project, 2015
Multi-Mission Optimally Interpolated Sea Surface Salinity (OISSS) Level 4 V1.0	Grid	SSS	0.25 × 0.25	Monthly	Melnichenko et al., 2021

2.12 MASKED SATELLITE SSS VALUES

A satellite SSS land mask extends outward from the coastline by 100 km for each month from 2015-2020. Due to the presence of the SSS land mask, coastal satellite-based SSS values are unavailable. **FIGURE 15** displays the area of the land mask contained within the OISSS Level 4 V2.0 product.

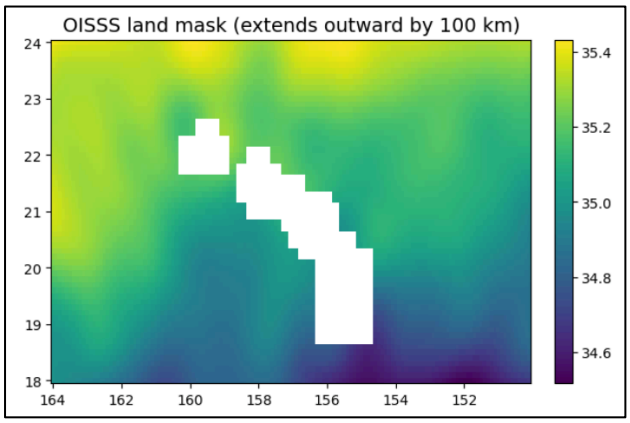

FIGURE 15

Land mask extending outward from the coastline by 100 km contained within the OISSS Level 4 V1.0 product.

2.13 SUBSTITUTION OF REGIONAL OCEAN MODELING SYSTEM (ROMS) SSS VALUES IN COASTAL AREAS COVERED BY THE SATELLITE SSS LAND MASK

Due to the presence of a satellite-based SSS land mask, coastal SSS measurements were unavailable; therefore, coastal SSS values from a Regional Ocean Modeling System (ROMS) for the Hawaiian region were used in coastal areas covered by the satellite SSS land mask (Friedrich et al., 2021). Coupled to the planktonic Carbon, Ocean Biogeochemistry and Lower Trophics (COBALT) ecosystem model, the ROMS is an assimilation model based on observations which simulates ocean physics and biogeochemical conditions for waters around the main Hawaiian Islands. The ROMS output incorporates physical forcing mechanisms such as rainfall rate, wind speed, etc. provided by a high-resolution Weather Regional Forecast (WRF) model. ROMS values are available at a 0.036˚ (approximately 4 km) horizontal resolution and the ROMS configuration includes a vertically stretched grid offering higher resolution at higher latitudes (Friedrich et al., 2021). In order to generate a map of Ω_{Ar} for the HIR, gridded values of SSS and SST were interpolated to a 0.1˚ Cartesian gride in order to match the resolution of interpolated grid points for satellite SSS and SST.

It has been shown that model results demonstrate good agreement between observed and simulated values at Station ALOHA as well as capturing seasonal cycles for many variables (Friedrich et al., 2021); additionally, there appears to be good agreement between the ROMS SSS and satellite SSS values for the open ocean. **FIGURE 16** below displays the average difference for each month between satellite and ROMS SSS values for the open ocean.

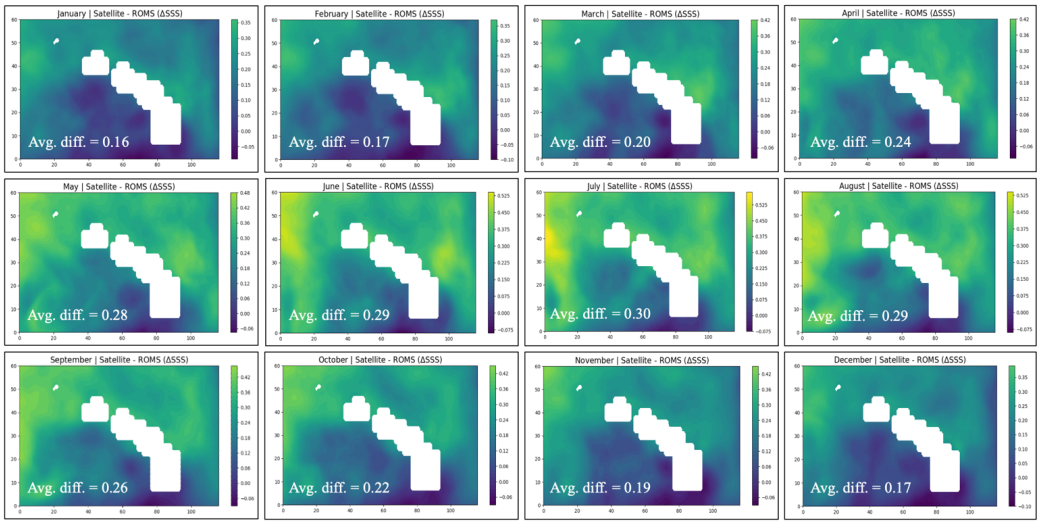

FIGURE 16

Average difference for each month between satellite and ROMS SSS values for the open ocean.

Average monthly differences between satellite and ROMS SSS values for the open ocean are greatest during the summer months from April-September. The mean value with respect to the average monthly differences is approximately 0.23˚C; although the uncertainty for OISSS values is approximately 0.2˚C, there appears to be relatively good agreement between satellite and ROMS SSS values for the open ocean; therefore, it is assumed that ROMS SSS values for the coastal areas would be similarly expressed.

2.14 INTEGRATING SATELLITE AND ROMS VALUES TO PRODUCE HYBRID MAPS OF Ω_{AR}

Following the interpolation of satellite and ROMS SSS values to a 0.1˚ Cartesian grid, values were then substituted into the empirical algorithms to calculate A_T and ΔpCO_2 across the HIR.

Latitude-dependent $pCO_{2,\,atm}$ values were retrieved from the GML database and since other variables are provided in a monthly format, $pCO_{2,\,atm}$ values for each month were averaged in order to produce a single monthly value. ΔpCO_2 and $pCO_{2,\,atm}$ values were additively combined to produce $pCO_{2,\,sw}$ values.

P, SSS, SST, $pCO_{2,\,sw}$ and A_T values were substituted into PyCO2SYS for the generation of Ω_{Ar} values across the HIR. The spatial resolution of the hybrid maps (produced using satellite and model-derived values) is 0.1˚ or approximately 11.1 km.

2.15 IN SITU DATASET UNCERTAINTIES

2.15.1 HAWAI‘I OCEAN TIME-SERIES (HOT)

In order to evaluate field precision, approximately 20% of the samples collected during each of the HOT cruises are used for duplicate or triplicate sample testing. The typical precision of SSS during replicate analyses using the same water sample is 0.0003 ‰; the typical precision of SSS during triplicate analyses is < 0.001 ‰; for purposes of approximating uncertainty, a bias of 0.0003 ‰ was assumed. The CTD temperature sensors are adjusted between each cruise and each of the HOT cruise data reports provide a set of suggested temperature corrections. For purposes of this study, the estimated average SST adjustment value is 0.0001 ˚C. The precision of A_T sample titrations is approximately 3 μeq kg^{-1} (information obtained from the Hawai‘i Ocean Time-series HOT-DOGS program affiliated with the University of Hawai‘i at Mānoa).

2.15.2 GLOBAL OCEAN DATA ANALYSIS PROJECT (GLODAP)

The Global Ocean Data Analysis Project (GLODAP) is a synthesized data product consisting of surface ocean biogeochemical measurements (Lauvset et al., 2022). GLODAP v2.2022 is an updated version of GLODAP v2.2021 (Lauvset et al., 2021). A crossover analysis for the GLODAP v2.2022 dataset includes a maximum bias estimate of 4 and 6 μmol kg^{-1} for A_T; these uncertainty values represent the maximum bias that exists between different instruments. A comprehensive uncertainty budget (consisting of a combination of bias and standard deviation of all measurements against an observable standard) is not provided or available. Given the absence of uncertainty information, a nominal uncertainty of 0.2% is assumed for all in situ A_T values collected from the GLODAP dataset; 0.2% of the average GLODAP A_T value (2,307.94 μmol kg^{-1}) is approximately 5 μmol kg^{-1} (Olsen et al., 2016). Uncertainties with respect to the input (forcing) data are unavailable (Land et al., 2019); uncertainty values for SST and SSS are estimated at 0.0001 ˚C and 0.003 ‰, respectively.

2.15.3 NATIONAL CORAL REEF MONITORING PROGRAM (NCRMP)

The uncertainty bias reported for in situ SST recorded from the CTD (ITS-90 scale) is 0.005 ˚C; the uncertainty bias reported for in situ SSS calculated from conductivity recorded by the CTD (using the Practical Salinity Scale of 1978) is 0.0005 S/m (Barkley et al., 2021); for purposes of this study, an uncertainty bias of 0.005 ‰ is assumed. The total uncertainty for A_T values was reported to be 0.1% (Barkley et al., 2021).

2.15.4 DISCRETE MEASUREMENTS

Discrete measurements collected from moored buoys surrounding O‘ahu were used in conjunction with NCRMP measurements to construct the subgroup #1 and subgroup #2 coastal algorithms for A_T calculations. For subgroup #1, discrete measurements were obtained from the Kāne‘ohe mooring beginning in February 2016 through January 2019; for subgroup #2, discrete

measurements were obtained from the Kilo Nalu and Ala Wai moorings beginning in February 2014 through December 2019.

Uncertainty values reported for bottle data collected from January 2016-September 2019 indicate an uncertainty bias of 0.05 (SBE) or 1% for conductivity (SSS), 0.01 ˚C for SST and 3 μmol kg^{-1} for A_T measurements (Knor et al., 2018). The same uncertainty approximations are assumed for all discrete measurements collected prior to January 2016.

2.15.5 SURFACE OCEAN CO_2 ATLAS (SOCAT)

SOCAT Version 2022 is a global product synthesized from many different data collection sources. A nominal uncertainty bias of 0.001 ˚C and 0.005 ‰ is assumed for SST and SSS. Accepted quality control flags include flags with an ID from A-D.

TABLE 6 below summarizes uncertainties for in situ measurements used to calculate open ocean A_T and ΔpCO_2 values.

TABLE 6. UNCERTAINTIES FOR IN SITU MEASUREMENTS USED TO CALCULATE OPEN OCEAN A_T AND ΔpCO_2 VALUES

Information regarding the open ocean data source, parameter, uncertainty and total uncertainty values for in situ measurements used to calculate open ocean A_T and ΔpCO_2 values.

Open ocean data source	Parameter	Uncertainty	Total uncertainty
HOT	SSS	0.0003 ‰	0.007 ‰
GLODAP V2.2022	SSS	0.005 ‰	
SOCAT v2.2022	SSS	0.005 ‰	
HOT	SST	0.0001 °C	0.001 °C
GLODAP V2.2022	SST	0.001 °C	
SOCAT v2.2022	SST	0.001 °C	
HOT	A_T	3 µmol kg^{-1}	5.83 µmol kg^{-1}
GLODAP V2.2022	A_T	0.2% or 5 µmol kg^{-1}	
SOCAT v2.2022	ΔpCO2	2 µatm	2 µatm

Table 7 below summarizes the uncertainty bias associated with each of the in situ measurements used to calculate coastal A_T and ΔpCO_2 values.

TABLE 7. UNCERTAINTIES FOR IN SITU MEASUREMENTS USED TO CALCULATE COASTAL A_T AND ΔpCO_2 VALUES

Information regarding the coastal data source, parameter, uncertainty and total uncertainty values for in situ measurements used to calculate coastal A_T and ΔpCO_2 values.

Subgroup	Coastal data Source	Parameter	Uncertainty	Total uncertainty
1	NCRMP	SSS	0.005 ‰	0.35 ‰
	Kāneʻohe (Discrete)	SSS	1%	
	NCRMP	SST	0.005 °C	0.01 °C
	Kāneʻohe (Discrete)	SST	0.01 °C	
	NCRMP	A_T	0.1%	3.76 µmol kg^{-1}
	Kāneʻohe (Discrete)	A_T	3 µmol kg^{-1}	
	SOCAT v2. 2022	ΔpCO_2	2 µatm	2 µatm
2	NCRMP	SSS	0.005 ‰	0.35 ‰
	Kilo Nalu (Discrete)	SSS	1 %	
	Ala Wai (Discrete)	SSS	1 %	
	NCRMP	SST	0.005 °C	0.015 °C
	Kilo Nalu (Discrete)	SST	0.01 °C	
	Ala Wai (Discrete)	SST	0.01 °C	
	NCRMP	A_T	0.1 %	3.77 µmol kg^{-1}
	Kilo Nalu (Discrete)	A_T	3 µmol kg^{-1}	
	Ala Wai (Discrete)	A_T	3 µmol kg^{-1}	
	SOCAT v2. 2022	ΔpCO_2	2 µatm	2 µatm
3	NCRMP	SSS	0.005 ‰	0.005 ‰
	NCRMP	SST	0.005 °C	0.005 °C
	NCRMP	A_T	0.1 %	2.26 µmol kg^{-1}
	SOCAT v2. 2022	ΔpCO_2	2 µatm	2 µatm
4	NCRMP	SSS	0.005 ‰	0.005 ‰
	NCRMP	SST	0.005 °C	0.005 °C
	NCRMP	A_T	0.1 %	2.27 µmol kg^{-1}
	SOCAT v2. 2022	ΔpCO_2	2 µatm	2 µatm

For the open ocean and for subgroups #1 and #2 in **TABLE 6** and **TABLE 7**, the total uncertainty value was calculated after taking the square root of the sum of the squares for each parameter within the dataset.

2.16 ALGORITHM UNCERTAINTIES

2.16.1 UNCERTAINTIES ASSOCIATED WITH THE A_T ALGORITHMS

Results from the OLS regression models used to derive the open ocean and coastal group algorithms were obtained for quantifying the A_T and ΔpCO_2 algorithm uncertainties. **FIGURE 17** below displays the algorithm uncertainty value for open ocean A_T calculations. The mean A_T value is 2,307.94 µmol kg^{-1} and the total uncertainty value associated with open ocean calculations is 7.59 µmol kg^{-1}.

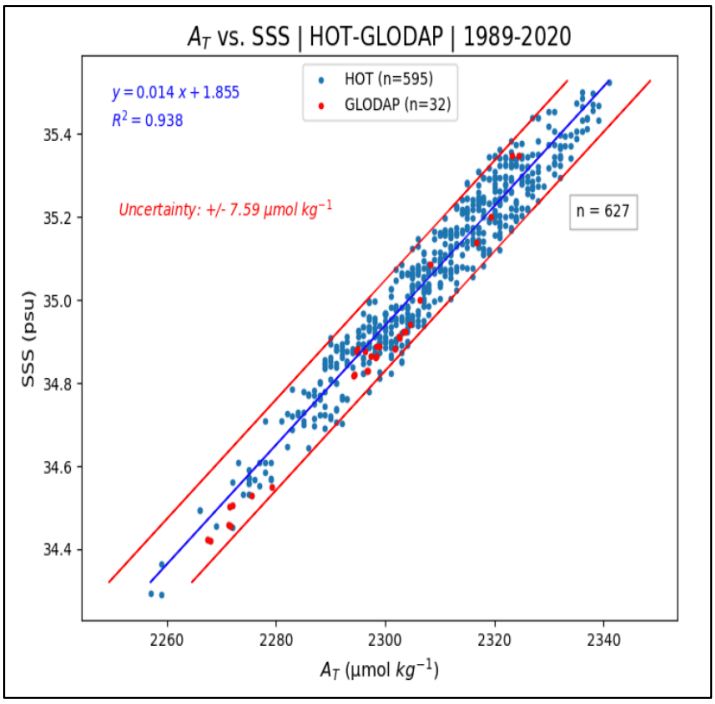

FIGURE 17

Results from the OLS regression model for the combined GLODAP v2.2022 and HOT datasets indicate a total algorithm uncertainty value of 7.59 µmol kg^{-1} (demarcated by red lines) for A_T calculations.

The same approach was applied for each of the coastal subgroups. **FIGURE 18** displays each of the values used to generate each of the coastal subgroup algorithms plotted against the open ocean values for comparison along with the uncertainty values for each of the coastal subgroup A_T algorithms.

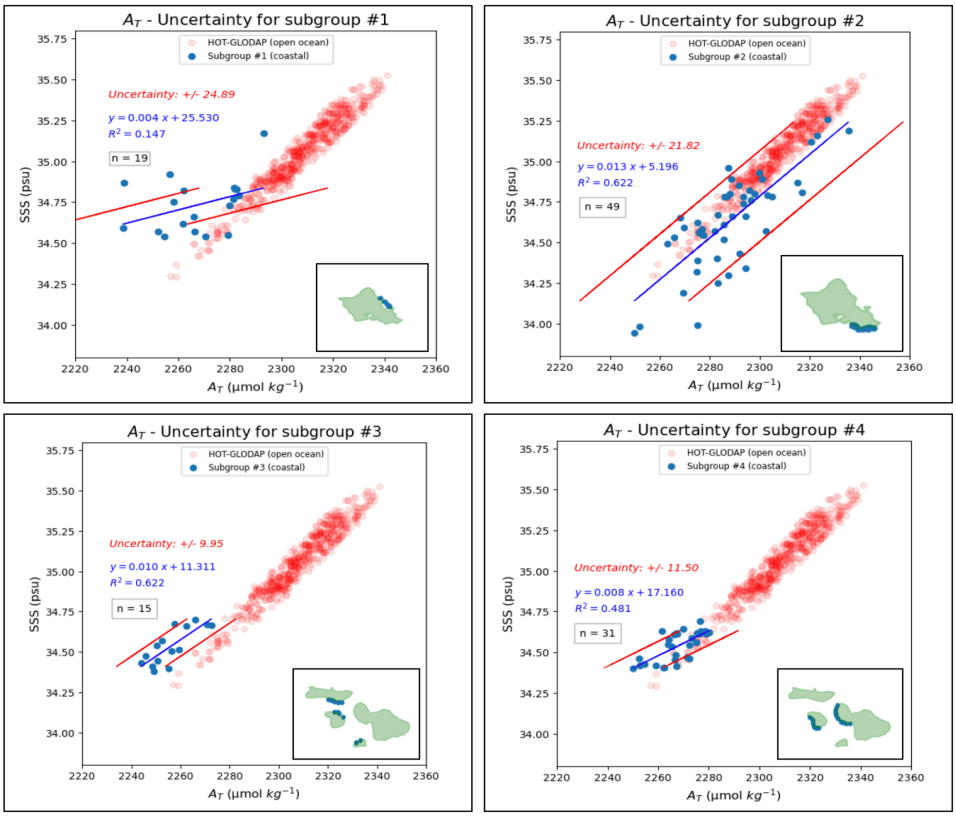

FIGURE 18

Coastal values used for generating the coastal subgroup algorithms for A_T calculations. Uncertainty values associated with each of the coastal subgroup A_T algorithms are provided. Inset maps displaying geographic locations of measurement collection sites are included for each subgroup.

The mean and total uncertainty values for each coastal subgroup A_T algorithm are summarized in **TABLE 8** below.

TABLE 8. MEAN AND TOTAL UNCERTAINTY VALUES FOR EACH COASTAL A_T SUBGROUP

Mean A_T and total uncertainty values for each coastal subgroup A_T algorithm are provided. Uncertainty values were obtained from the results of each OLS regression model.

Coastal subgroup	Mean A_T value	Total uncertainty
1	2267.86 μmol kg^{-1}	24.89 μmol kg^{-1}
2	2288.46 μmol kg^{-1}	21.82 μmol kg^{-1}
3	2256.12 μmol kg^{-1}	9.95 μmol kg^{-1}
4	2267.86 μmol kg^{-1}	11.50 μmol kg^{-1}

2.16.2 UNCERTAINTIES ASSOCIATED WITH THE ΔPCO_2 ALGORITHMS

FIGURE 19 below displays the algorithm uncertainty value for open ocean ΔpCO_2 calculations. The mean ΔpCO_2 value is -5.38 μatm and the total uncertainty associate with open ocean calculations is 22.10 μatm.

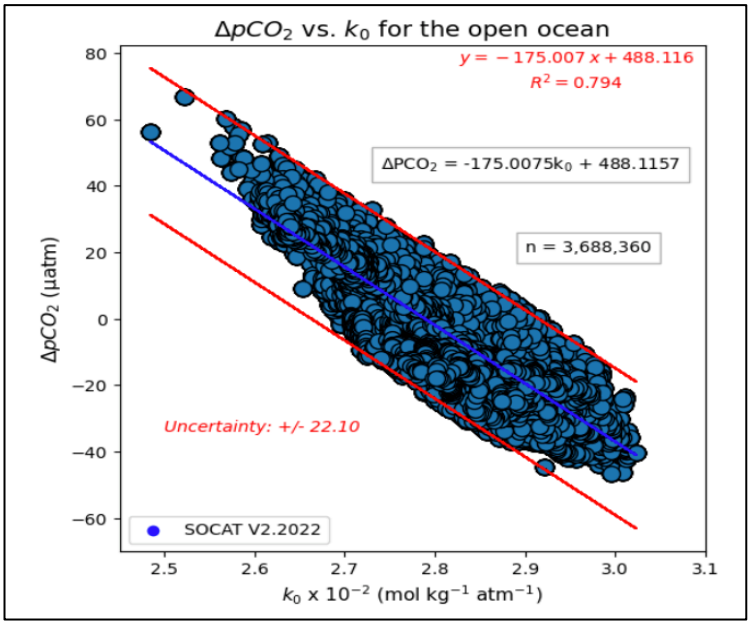

FIGURE 19

ΔpCO_2 vs. k_0 for the open ocean. The mean ΔpCO_2 value is -5.38 µatm and the total uncertainty associated with open ocean calculations is 22.10 µatm.

FIGURE 20 displays the uncertainty values associated with each of the subgroups used to develop the coastal ΔpCO_2 algorithms. It is important to note that for subgroups #3 and #4, the uncertainty value for subgroup #2 is assigned since the subgroup #2 algorithm was used due to a lack of available measurements for all zones in subgroups #3 and #4. The mean ΔpCO_2 value for subgroup #1 and #2 is 38.37 and 8.13 µatm, respectively; the total uncertainty associate with subgroup #1 and #2 calculations is 91.95 and 69.33 µatm. For coastal subgroups #3 and #4, the subgroup #2 algorithm was assigned for ΔpCO_2 calculations.

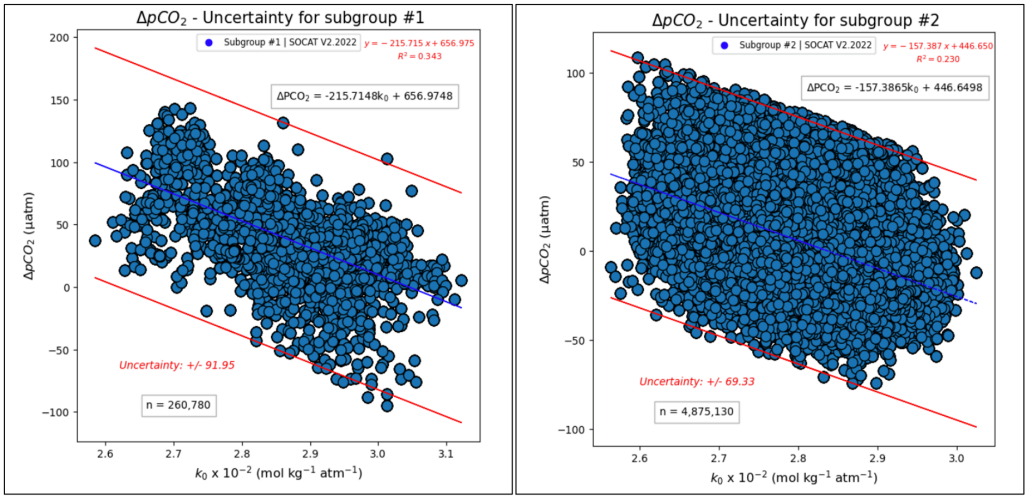

FIGURE 20

Uncertainty values associated with each of the subgroups used to develop the coastal ΔpCO_2 algorithms.

The mean and total uncertainty values for each coastal subgroup ΔpCO_2 algorithm are summarized in **TABLE 9** below.

TABLE 9. MEAN AND TOTAL UNCERTAINTY VALUES FOR EACH COASTAL ΔPCO_2 SUBGROUP

Uncertainty values were obtained from the results of each OLS regression model. Note: subgroups #3 and #4 assume the subgroup #2 mean and total uncertainty values due to a lack of measurements for all zones in subgroups #3 and #4.

Coastal subgroup	Mean ΔpCO_2 value	Total uncertainty
1	38.37 µatm	91.95 µatm
2	8.13 µatm	69.33 µatm
3	8.13 µatm	69.33 µatm
4	8.13 µatm	69.33 µatm

2.17 SATELLITE DATASET UNCERTAINTIES

2.17.1 MULTI-MISSION OPTIMALLY INTERPOLATED SEA SURFACE SALINITY (OISSS)

The Multi-Mission Optimally Interpolated Sea Surface Salinity (OISSS) product combines global observations from NASA's Aquarius/SAC-D and Soil Moisture Active-Passive (SMAP) missions. All satellite SSS data from January to March 2015 originated from the Aquarius satellite; products are available on a 0.25˚ grid following Optimum Interpolation analysis (Melnichenko et al., 2016). The OISSS product also includes SMAP satellite-based SSS data from Remote Sensing Systems (RSS); SSS fields are generated from Level-2 swath data using the OI algorithm. Further adjustments are made to SMAP SSS fields through spatial filters, reducing small-scale noise and to ensure consistency across the time series. During an overlap period from April-May 2015, data from SMAP and Aquarius/SAC-D satellites were averaged together. A gap in SMAP observations occurs from June-July 2019 while the satellite was in safe mode; to fill the gap in SSS observations, measurements from ESA's Soil Moisture and Ocean Salinity (SMOS) satellite were used (Melnichenko et al., 2021).

The consistency and accuracy of the OISSS product has been evaluated against SSS measurements from Argo floats and mooring buoys. The root-mean-square-difference (RMSD) between the Aquarius/SMAP OISSS dataset and global in situ data is approximately 0.2 psu (Melnichenko et al., 2016). Uncertainty estimates incorporate random and systematic uncertainties, Argo data sampling errors on gridded map scales and mapping errors (Meissner et al., 2019).

2.17.2 MULTI-SCALE ULTRA-HIGH RESOLUTION (MUR) SST ANALYSIS

Each of the empirically derived algorithms were forced with monthly mean satellite SST values collected from the Multi-scale Ultra-high Resolution (MUR) SST Analysis. These products are provided by the NASA Jet Propulsion Laboratory (JPL) and are supported by the NASA

MEaSUREs program. The MUR SST monthly means are created by the National Oceanic and Atmospheric Administration (NOAA), National Marine Fisheries Service (NMFS), Southwest Fisheries Science Center (SWFSC), Environmental Research Division (ERD) and are based on daily MUR SST values. The source dataset consists of JPL MUR climatology products and multi-sensor L4 Foundation SST analysis products; this dataset is part of the Group for High-Resolution Sea Surface Temperature (GHRSST) project (JPL, 2015). Global SST values from this dataset are provided at a 0.01˚ resolution and contains a bias of approximately 0.07 ˚C (Chin et al., 2017).

2.17.3 REGIONAL OCEAN MODELING SYSTEM (ROMS) SSS VALUES

For areas otherwise covered by the satellite land mask, ROMS SSS values were used to calculate Ω_{Ar}. ROMS SSS values contain a bias of 0.001 ‰ for SSS values and 0.28 ˚C for SST values (Friedrich et al., 2020).

2.18 PYCO2SYS

Uncertainty propagation is calculated internally by PyCO2SYS when provided with an appropriate input argument. Uncertainty calculations are carried out using **Equation (14)** below:

$$\sigma^2(r) = \Sigma(\partial r/\partial a_i)^2 \, \sigma^2(a_i) \qquad \textbf{(14)}$$

σ represents the uncertainty as a standard deviation. **Equation (14)** is valid as long as all uncertainties are independent and as long as there are no instances of co-variance (Humphreys et al., 2022).

2.19 HYBRID MAPS OF Ω_{AR}

Hybrid maps with calculated Ω_{Ar} values were constructed using satellite SSS and SST and ROMS SSS values.

Following the entry of parameter uncertainty values in PyCO2SYS for A_T, $pCO_{2,sw}$, SSS and SST for the open ocean and for each coastal subgroup, the total uncertainty values are 0.12, 0.48 and 0.36 for the open ocean, subgroup #1 and subgroups #2-#4 Ω_{Ar} calculations.

2.20 LONG-TERM TRENDS IN Ω_{AR}

In order to determine the long-term trend in Ω_{Ar} across the HIR, a plot containing monthly mean Ω_{Ar} values was generated for all months from 2015-2020 (**FIGURE 21**).

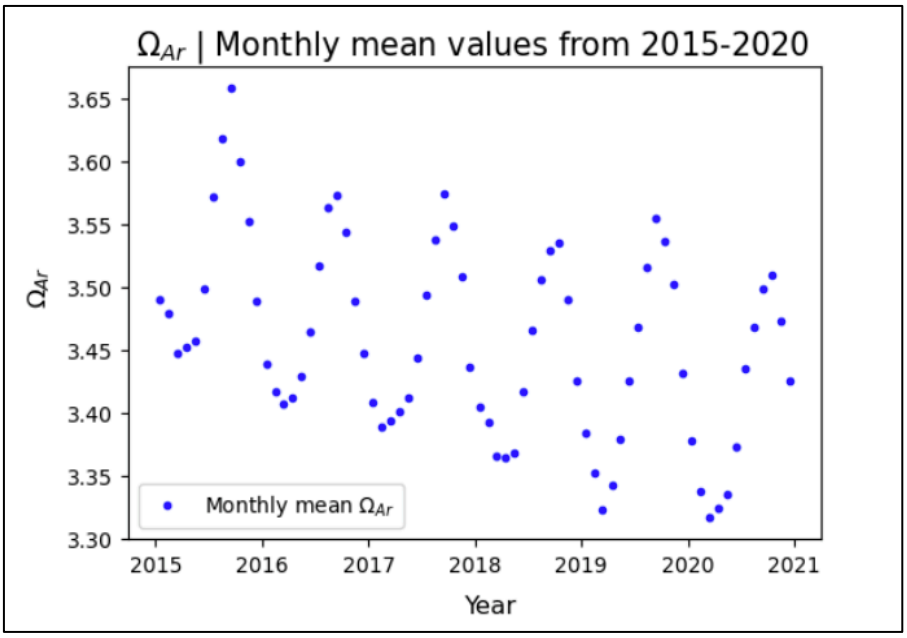

FIGURE 21

Monthly mean Ω_{Ar} values for all months from 2015-2020.

An OLS regression model consisting of sine and cosine components was used for fitting monthly mean Ω_{Ar} values. The model establishes a trendline based on dual fits between the monthly mean Ω_{Ar} values and a sine wave component along with the monthly mean Ω_{Ar} values and a cosine wave component. Since the frequency of the sinusoid is a known value, only amplitude and phase are determined by the fit which yield the cosine and sine coefficients; the OLS model

determines the best combination of model components to describe the dataset while simultaneously finding a solution that most greatly reduces model residuals. Results from the OLS model fit along with corresponding residual values are displayed in **FIGURE 22** below.

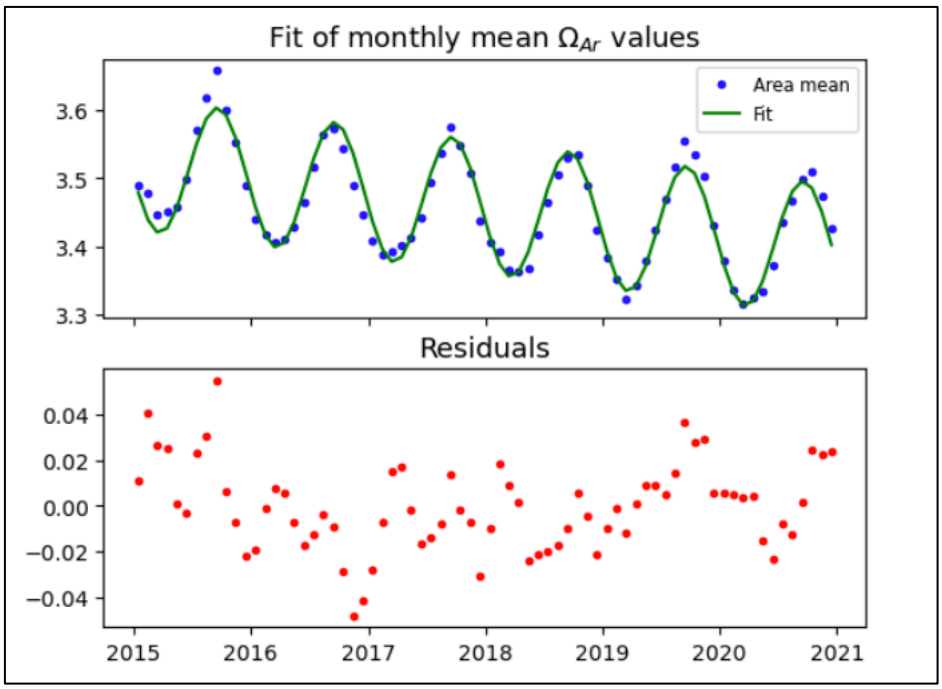

FIGURE 22

Results from the OLS model fit (top) with corresponding residual values (bottom).

Components of the model matrix were constructed in order to derive sine and cosine coefficients for determining the rate of change per decade. Linear regression techniques were used to plot a decadal trendline using fitted model parameters.

In order to establish an uncertainty value for long-term trends in Ω_{Ar}, individual uncertainty values for A_T, $pCO_{2,\,sw}$, SST and SSS were entered into PyCO2SYS. The total uncertainty value generated for the open ocean was determined to be 0.12 and is displayed against the decadal trendline in **FIGURE 23**.

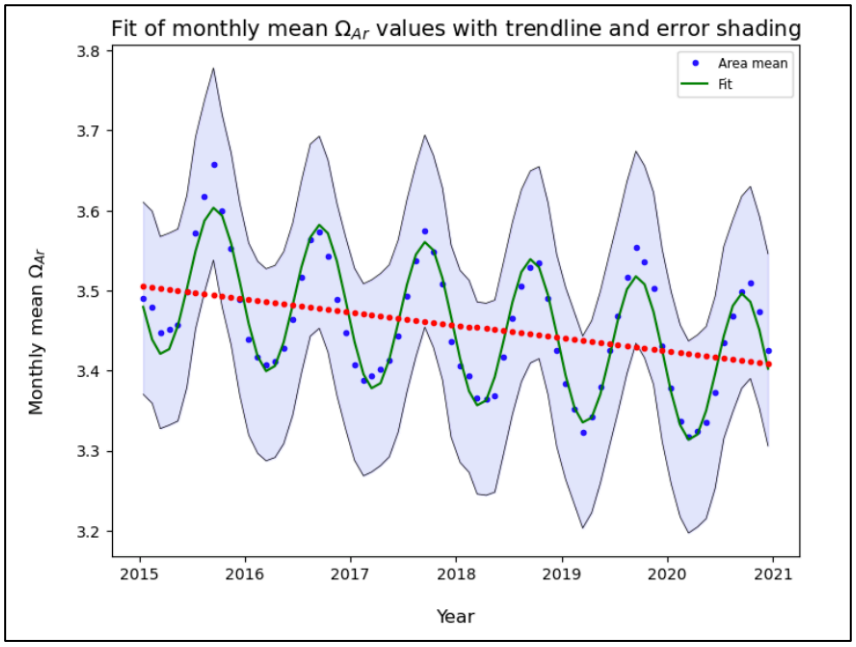

FIGURE 23

Fit of monthly mean Ω_{Ar} values with decadal trendline and error shading representing a value deviation of 0.12.

CHAPTER 3. RESULTS

3.1 INFLUENCE OF CORALS ON THE A_T VS. SSS RELATIONSHIP

The first hypothesis suggests that the presence of coral reefs changes the slope of the total alkalinity (A_T) vs. sea surface salinity (SSS) relationship. When compared to the tightly coupled linear A_T vs. SSS relationship for the open ocean (**FIGURE 4**), coastal A_T vs. SSS relationships are more variable and appear to vary with coral coverage patterns. Consider each of the coastal subgroup A_T vs. SSS plots – based on the results from this study, a correlation exists between the percentage of coral coverage and the A_T and/or slope values.

3.2 ZONAL DIFFERENCES BASED ON THE CLIMATOLOGICAL ANNUAL CYCLE IN Ω_{AR}

To quantify east-west differences in Ω_{Ar}, values across the HIR, month-based averages of Ω_{Ar} were calculated across the HIR from 2015-2020. For example, all of the calculated Ω_{Ar} values for the month of January were averaged together at each grid point and displayed as a single map representing an average of all Ω_{Ar} values for the month of January. According to a map of the canonical current system around the MHI (**FIGURE 24(A)**; Powell, B. S. (2017)), the easternmost extent of the HLCC occurs at approximately 157˚W; therefore, a meridional transect was inserted at 157˚W to demarcate the boundary separating the east and west components of the study domain; **FIGURE 24(B)** displays the average month-based Ω_{Ar} values calculated for the east and west components of the study domain.

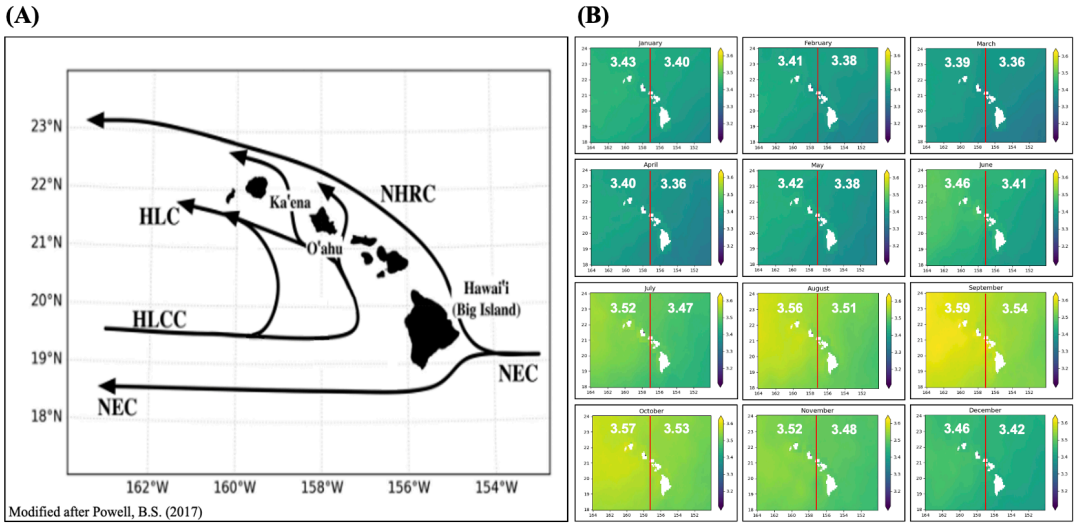

FIGURE 24

(A) Map of the canonical current system around the MHI from Powell, B. S. (2017). (B) A meridional transect is inserted at 157˚W to demarcate the easternmost extent of the HLCC and serves as the boundary separating the east and west components of the study domain. Average month-based Ω_{Ar} values calculated for the east and west components of the study domain are included.

Based on the results in **FIGURE 24(B)** – from January to March, value differences are approximately 0.03; the greatest difference in values (0.05) is observed during the month of August. The average difference between east and west values is approximately 0.04.

3.3 ASSESSMENT OF ALGORITHM PARAMETER SENSITIVITIES AND EFFECTS ON CALCULATED Ω_{AR} VALUES

Monthly averages of SSS, SST, $pCO_{2,\,sw}$ and A_T were included as input parameters in PyCO2SYS in order to calculate surface ocean Ω_{Ar} for the HIR. To determine the parameter that has the greatest effect on surface ocean Ω_{Ar} for the HIR, the sensitivities of each of the four carbonate system input parameters – A_T, $pCO_{2,\,sw}$, SSS and SST – were investigated. All four of these input parameters were considered independently in order to identify the parameter with the

greatest influence on calculated surface ocean Ω_{Ar} values – specifically as it relates to the spatiotemporal range established for this investigation.

Each of the four input parameters recorded for February 2017 were autonomously modified. For example, only the monthly mean SSS values recorded for February 2017 were modified to reflect September 2017 values; the corresponding change in Ω_{Ar} reveals the effect of SSS on Ω_{Ar}; similar procedures were followed for SST, $pCO_{2,\,sw}$ and A_T to observe how changes to each parameter contribute to the change in Ω_{Ar}. The change in Ω_{Ar} following each single parameter modification is referred to as $\Delta\Omega_{Ar}$, which reflects the difference between the new Ω_{Ar} value and the Ω_{Ar} value recorded for February 2017.

Sites H (northeast O‘ahu) and I (northwest Moloka‘i) were selected for comparison. Results from this comparison are provided in **FIGURE 25**. For Site H, upon recalculating Ω_{Ar} after implementing stepwise changes to each of the four input parameters, the greatest $\Delta\Omega_{Ar}$ value of 0.36 occurs with the modification of SST, which is sequentially following by $pCO_{2,\,sw}$ (-0.19), A_T (-0.05) and SSS (~0). Similarly, for Site I, the greatest $\Delta\Omega_{Ar}$ value occurs with the modification of SST and reflects the same order of influence for $pCO_{2,\,sw}$ (-0.15), A_T (0.05) and SSS (0.01). It is important to note that while changes in SST appear to produce a much larger seasonal cycle, the magnitude of this change is offset by negative corrections from $pCO_{2,\,sw}$ and A_T.

	Feb. 2017	Sep. 2017	New Ω_{Ar}	$\Delta\Omega_{Ar}$
SSS	34.61	34.83	3.12	~0
A_T	2286.98	2264.29	3.06	-0.05
Seawater pCO_2	422.79	466.12	2.92	-0.19
SST	23.99	27.36	3.47	0.36

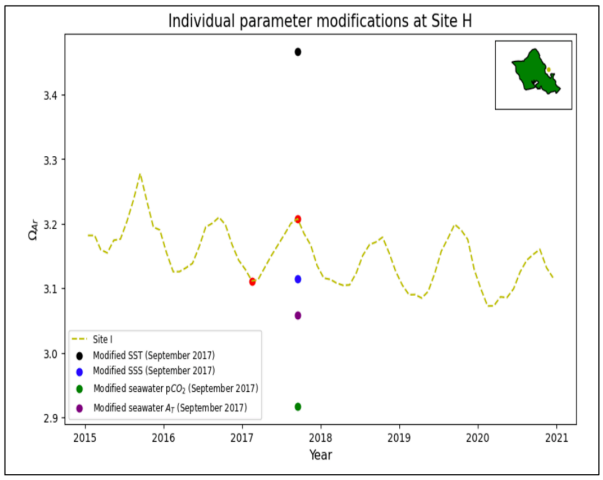

	Feb. 2017	Sep. 2017	New Ω_{Ar}	$\Delta\Omega_{Ar}$
SSS	34.52	34.83	3.36	0.01
A_T	2273.68	2293.0	3.40	0.05
Seawater pCO_2	377.64	406.19	3.20	-0.15
SST	24.38	27.34	3.68	0.32

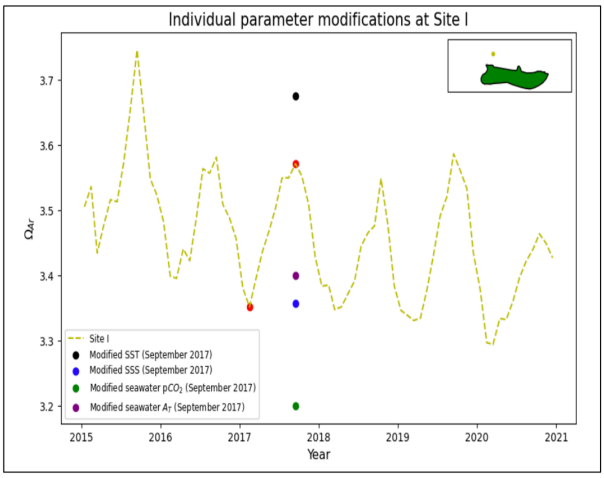

FIGURE 25

Results from single parameter value modifications from February to September 2017 at Sites H (northeast O‘ahu) and I (northwest Moloka‘i). The change in Ω_{Ar} from February 2017 to September 2017 following each single parameter modification is referred to as $\Delta\Omega_{Ar}$, which reflects the difference between the new Ω_{Ar} and the Ω_{Ar} value recorded for February 2017. Value differences were evaluated to identify the parameter with the greatest influence on consequent Ω_{Ar} values.

A similar analysis was performed for the open ocean at Station ALOHA (**FIGURE 26**). Similar to the results obtained for Sites H and I, the greatest $\Delta\Omega_{Ar}$ value at Station ALOHA occurs with the modification of SST (0.38) and reflects the same order of influence for $pCO_{2,\,sw}$ (-0.18), A_T (-0.02) and SSS (~0).

	Feb. 2017	Sep. 2017	New Ω_{Ar}	$\Delta\Omega_{Ar}$
SSS	34.93	34.81	3.40	~0
A_T	2300.49	2291.47	3.38	-0.02
Seawater pCO_2	371.33	405.42	3.22	-0.18
SST	23.81	27.28	3.79	0.38

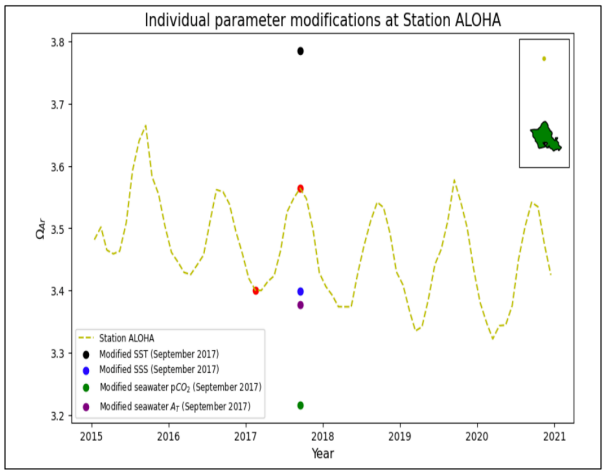

FIGURE 26

Results from single parameter value modifications from February to September 2017 at Station ALOHA. The change in Ω_{Ar} from February 2017 to September 2017 following each single parameter modification is referred to as $\Delta\Omega_{Ar}$, which reflects the difference between the new Ω_{Ar} value and the Ω_{Ar} value recorded for February 2017. Value differences were evaluated to identify the parameter with the greatest influence on consequent Ω_{Ar} values.

3.4 LONG-TERM TRENDS IN Ω_{AR}

In order to determine the long-term trend in Ω_{Ar} across the HIR, a plot containing monthly mean Ω_{Ar} values was generated for all months from 2015-2020 (**FIGURE 21**). Results from a linear fit produced by an OLS model using fitting techniques (**FIGURE 22**) reveal a mean value of 3.46 and a decadal trend of -0.21. Since the open ocean algorithm represents the primary algorithm used across the domain (used across 99% of the total domain area), **FIGURE 23** displays the decadal trendline along with error shading reflecting the uncertainty associated with open ocean values (0.12).

To determine the uncertainty with respect to the decadal trendline, a OLS regression model was constructed and contained monthly mean Ω_{Ar} values and model matrix components. Uncertainty with respect to the decadal trendline was calculated to be 0.02. Covariance testing indicated that

each of the model components were independent and the correlation coefficient (R^2) as determined by the model was 0.937.

3.5 HYBRID MODEL EVALUATION

3.5.1 MONTHLY MEAN VALUE COMPARISONS FOR A_T AND Ω_{AR} AT STAION ALOHA

Hybrid model results were compared with HOT values using time-series plots containing monthly mean values for A_T and Ω_{Ar} at Station ALOHA (**FIGURE 27**). ROM values are also included for reference. A_T values produced by the hybrid model appear to share good agreement with HOT values; the average difference is approximately 3.06 ± 7.68 µmol kg^{-1}. Since the standard deviation of the difference (7.68 µmol kg^{-1}) is larger than the average difference, there is no statistically significant bias between the hybrid and HOT values. Ω_{Ar} values produced by the hybrid model share similarities with respect to the seasonal cycles produced from HOT values; the average difference between the hybrid model and HOT Ω_{Ar} values is approximately 0.08 ± 0.05. In this case, the mean is larger than the standard deviation (0.05), but still larger than the total uncertainty value for hybrid model open ocean values (0.12). The average $\Delta\Omega_{Ar}$ is also close to the HOT Ω_{Ar} uncertainty value (0.07), which suggests there is likely no statistically significant bias.

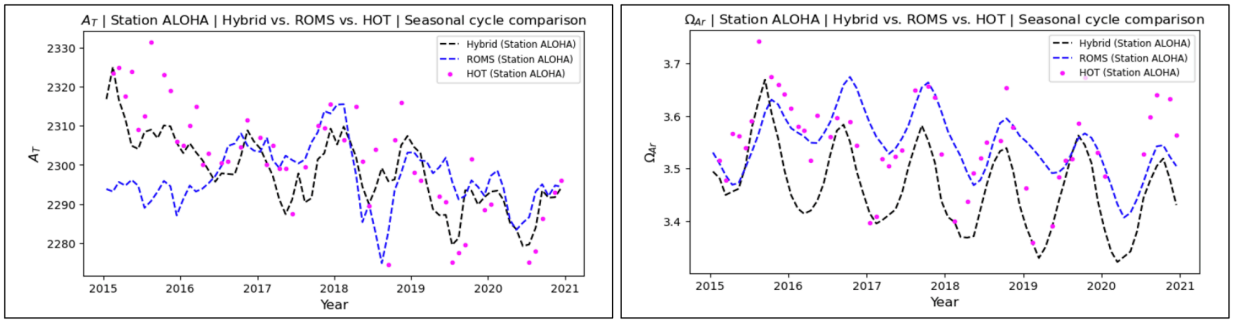

FIGURE 27

Hybrid model results (black line) compared with ROM (blue line) and HOT values (pink dots) using time-series plots containing monthly mean values for A_T and Ω_{Ar} at Station ALOHA.

3.5.2 COMPARISON OF DECADAL TRENDS IN Ω_{AR} BETWEEN THE HYBRID AND ROMS VALUES

Similar methods were followed as discussed in **2.20 LONG-TERM TRENDS IN Ω_{AR}** for generating a decadal trendline using ROMS values. Compared to the slope of the decadal trendline produced from hybrid values (-0.21), the ROMS model produced a slightly lower slope of -0.16, which is not significantly different.

CHAPTER 4. DISCUSSION

4.1 CORAL AND COASTAL A_T VS. SSS RELATIONSHIPS

Coastal A_T vs. SSS relationships appear to vary with percent coral coverage. Consider each of the coastal subgroups – for subgroup #1, each of the clusters are defined by a tier value of 3, indicating there are greater percentages of corals (> 50%) in these areas; when compared with the A_T vs. SSS relationships for all other subgroups (with average tier values of 1, 2 and 2.5), subgroup #1 contains the most noise. Additionally, the average A_T value for subgroup #1 is 2267.86 μmol kg^{-1} which is less than the average A_T value (2307.94 μmol kg^{-1}) for the open ocean. The average tier value assignment for subgroup #3 is 2.5; although the A_T vs. SSS slope values are nearly the same (differ by 0.001) between subgroup #3 and the open ocean, the average A_T value (2288.46 μmol kg^{-1}) for subgroup #3 is less than the average open ocean A_T value across similar SSS ranges. Each of the clusters in subgroup #4 contain tier 2 values; when comparing A_T vs. SSS relationships between subgroup #4 and open ocean values – although approximately 50% of values overlap, the A_T vs. SSS slope is shallower for subgroup #4 than it is for the open ocean; the average A_T value for subgroup #4 is 2267.86 μmol kg^{-1}, the same as was calculated for subgroup #1.

Although there are significant differences between coastal and open ocean algorithm performances across the region, these findings emphasize the differences that exist between open ocean and coastal water A_T vs. SSS relationships, the latter of which are likely influenced by coral reef activities or other nearshore processes.

4.2 ZONAL DIFFERENCES IN Ω_{AR} VALUES

It appeared likely that the transport of warmer water from west to east across the Pacific via the HLCC would introduce water with higher Ω_{Ar} values; to further elaborate, SST values are higher to the west and with higher temperatures, there is a decrease in CO_2 solubility. The reactions that occur between CO_2 and seawater to produce carbonic acid decreases, which decreases the

amount of free hydrogens released after carbonic acid dissociates to H^+ and HCO_3^-. Ultimately, there are less H^+ ions available to bind with free CO_3^{2-} compounds. The increased availability of CO_3^{2-} ions will result in increased Ω_{Ar} values as they bind to calcium (Ca^{2+}) ions in seawater. It appears to be warmer on the west side of O'ahu, therefore it seemed likely that Ω_{Ar} values would be higher on the western portion of the study domain. The average difference between east and west values was calculated to be 0.04; while zonal differences may occur, these differences are not statistically significant (< 0.12) and do not conclusively support hypothesis #2.

4.3 ANALYSES OF ALGORITHM PARAMETER SENSITIVITIES

For Sites H and I, changes in SST produced the largest $\Delta\Omega_{Ar}$ value; therefore, changes in SST appears to have the greatest effect on calculated surface ocean Ω_{Ar} values. From February to September 2017, $pCO_{2,\,sw}$ increased at Sites H and I by 43.33 and 28.55, which may be result from a warming of the waters and thermodynamic changes in the carbon system equilibrium (Takahashi et al., 2002). The decrease in A_T at Site H, located in a tier 3 region, is likely due to biological sequestration of CO_3^{2-} by marine calcifiers (such as coral). SSS appears to have the smallest effect on resulting Ω_{Ar} values, increasing $\Delta\Omega_{Ar}$ by ~0 at Site H and 0.01 at Site I. Similarly, SST appears to have the greatest effect on calculated Ω_{Ar} values for the open ocean followed by $pCO_{2,\,sw}$, A_T and SSS using the empirically derived algorithms.

SST appears to have the greatest effect on calculated Ω_{Ar} values due to the effects of SST on CO_2 solubility and $pCO_{2,\,sw}$ concentrations. In **Equation (5)**, warmer SSTs would reduce the denominator, K_{sp}, which increases the ratio of the numerator to denominator and increases Ω_{Ar}. SST has the opposite effect on $pCO_{2,\,sw}$; as SST increases, $pCO_{2,\,sw}$ increases. Increasing $pCO_{2,\,sw}$ decreases the concentration of CO_3^{2-}; since the concentration of CO_3^{2-} is in the numerator, this leads to a decrease in Ω_{Ar} values. In this case, SST effects on $pCO_{2,\,sw}$ only effect the numerator and not the denominator, but are smaller than the direct effect of increasing SST on the denominator leading to a net effect of increasing Ω_{Ar}.

4.4 LONG-TERM DECREASE IN Ω_{AR} AND CORAL TOLERANCE LIMITS

The continuation of anthropogenic emissions to the atmosphere will likely impact the marine carbonate system and affect the local marine environments around Hawai‘i. As atmospheric CO_2 concentrations continue to rise and as surface ocean Ω_{Ar} concentrations continue to decrease, it's likely that long-term, progressive decreases in coral calcification rates and growth will occur. Additionally, differences in species-level responses could lead to changes in reef community structure (Guinotte et al., 2003). The significance of these applications are observed through impacts most notably recognized among calcifying organisms such as corals. Decreased calcification rates and modifications to the food web structure has the potential to affect productivity and ocean biodiversity (Kleypas et al., 2006). Since coral Ω_{Ar} tolerance limits are influenced by factors such as geographic and species-level differences, it is assumed that a coral Ω_{Ar} tolerance limit of about 3.0 will likely induce coral stress in the shallow coastal waters around the MHI (Guan et al., 2015).

While a nonlinear decrease in Ω_{Ar} may occur, a roughly approximated linear extrapolation based on a decadal decrease of -0.21 indicates that monthly mean Ω_{Ar} values will drop below a value of 3.0 by 2041, supporting the supposition that Ω_{Ar} values will cross the coral threshold within the next 30 years. Following a similar approach using ROMS values and based on a decadal decrease of -0.16, monthly mean Ω_{Ar} values are projected to drop below a value of 3.0 by 2055. A 10% to 20% reduction in Ω_{Ar} represents a significant deficiency for calcifying organisms like corals. While monthly mean Ω_{Ar} values are projected to decrease below a value of 3.0 by 2041, the primary effects caused by reductions in Ω_{Ar} include weakened skeletal structures, decreases in coral cover and increased susceptibility to erosion (Kleypas et al., 1999).

4.5 QUANTIFYING ADDITIONAL UNCERTAINTIES

Biologically-induced perturbations of the marine carbonate system could result in uncertainties in the proxy estimates. The degree of photosynthesis and respiration occurring at or near the sea surface will affect the marine carbonate system through the removal or addition of CO_2 (Land et

al., 2015). The level of biological activity can be approximated for using estimations of chlorophyll and/or nitrate but unfortunately, these values were extremely limited within the study domain and were unable to be used for widespread approximations of biological activity at the ocean surface.

Due to resolution differences between satellite SSS and SST measurements and SSS values from the ROMS, interpolation techniques were utilized in order to rebroadcast each dataset onto a 0.1˚ Cartesian grid. Each dataset was interpolated prior to manipulation via algorithm forcing. While this interpolation technique enhanced the resolution of the satellite SSS dataset (originally 0.25˚), it consequently reduced the original resolution of the satellite SST (0.01˚) and ROMS SSS (0.036˚) datasets. The uncertainty associated with these interpolations is unknown, however it is assumed that these uncertainties are negligible.

4.6 ALGORITHM VALIDATION

Assessing the effectiveness of regionally constructed empirical algorithms requires quantifying Ω_{Ar} predictability for each region. In order to assess this approach, in situ patterns of surface water carbonate system variables must be reproducible from satellite-based measurements and calculations. Unfortunately, due to the limited availability of in situ measurements, all available measurements were used to construct each of the empirical algorithms; therefore, these measurements were unable to be used for algorithm validation.

4.7 HYBRID MODEL EVALUATION

Based on the results provided in **FIGURE 27**, hybrid model A_T values appear to be in good agreement with A_T values at Station ALOHA; the average difference in values is approximately 3.06 ± 7.68 μmol kg^{-1}. The slight offset in Ω_{Ar} values (0.08 ± 0.05), however, between the hybrid and HOT values is minimal and as such, does not indicate a significant difference between the hybrid and HOT values. The slight offset could be due to small differences in $pCO_{2,\,sw}$; the average difference in values is approximately 12.35 ± 6.65 μmol kg^{-1}. Although differences in

$pCO_{2,\,sw}$ may be the primary cause of this offset, additional investigations are needed. Additionally, the difference between the slope values of the decadal trendline for Ω_{Ar} between the hybrid and ROM (0.05) is minimal but may be indirectly related to differences in $pCO_{2,\,sw}$ values; additionally, Ω_{Ar} uncertainties between the HOT and hybrid models could be simultaneously contributing to this difference, however additional studies are needed before establishing conclusive findings.

CHAPTER 5. CONCLUSIONS

This study demonstrated the effectiveness of utilizing satellites for evaluating OA across the HIR. Methods for downscaling satellite measurements could be similarly applied to other regions across the globe. One of the caveats to this approach, however, is a reliance on the availability of in situ measurements for synthesizing empirical algorithms.

5.1 THE NEED FOR ADDITIONAL IN SITU MEASUREMENTS ACROSS THE HIR

Empirical algorithms developed from in situ measurements will require periodic retraining in order to more accurately predict A_T, ΔpCO_2 and ultimately, Ω_{Ar} values in waters across the HIR. Unfortunately, recurrent measurements of A_T and ΔpCO_2 are limited across the HIR (especially for coastal areas (i.e., DDZs). With more frequent measurements of parameters such as A_T and ΔpCO_2, empirically-derived algorithms can be generated from a larger pool of in situ values.

While many oceanographic variables are more consistently observed in places like Station ALOHA, more frequent measurements of other in situ parameters (i.e., chlorophyll, nitrate, calcification rates, etc.) would have greatly contributed to this study. Use of calcification rates instead of estimated percentages of coral coverage, for example, may prove to be a more accurate method of estimating the effects of calcification on the A_T vs. SSS relationship. Additionally, carbon concentrations are strongly affected by surrounding biological activity (i.e., planktonic primary production), which is related to the amount of chlorophyll or nitrate located at the surface ocean. For some near-shore and high nutrient marine environments, these types of measurements may be used to enhance the predictability of marine carbonate chemistry parameters than can be used to calculate Ω_{Ar} with PyCO2SYS.

5.2 IMPLEMENTATION STRATEGIES

Access to near real-time oceanographic data has the potential to revolutionize current research strategies; by forcing empirical algorithms with near real-time satellite measurements, valuable

information can be obtained and used to direct the placement of autonomous platforms around the MHI; for example, moored buoys could be strategically placed (i.e., in areas with lower Ω_{Ar} values) as a way to closely monitor changes in surface ocean biogeochemistry in certain locations. Furthermore, understanding biogeochemical changes at a local level will support policies that govern and sustain fisheries. These kinds of data can be used to inform companies and corporations focused on maintaining and improving environmental health; additionally, existing policies and guidelines established by government agencies (i.e., NOAA) could be revised and/or updated based on new environmental data.

5.3 IMPORTANCE OF DOWNSCALING REMOTE MEASUREMENTS FOR REGION-SPECIFIC ANALYSES

Satellite-based estimations of surface ocean parameters like Ω_{Ar} are useful for widespread spatial extrapolations of surface ocean properties. Through increased coverage over extended temporal and spatial scales, assessments using satellite data will improve the precision of carbon exchange estimates (Lohrenze et al., 2018); through advancements in technology, widespread coastal satellite SSS fields and/or higher resolution products may become available; the need for high resolution SSS fields and/or higher resolution products may become available; the need for high resolution satellite SSS output is critical for determining small-scale changes occurring within targeted areas (such as the HIR). These small-scale changes will allow scientists to explore how regional effects resulting from OA are likely to impact the local economy, both from a biological and economic perspective.

Given the limitations imposed by sparse in situ measurements, methods for developing regionally tuned algorithms from in situ observations for mapping surface ocean parameters like Ω_{Ar} are important when it comes to small-scale climatological evaluations; additionally, methods used for developing satellite algorithms from in situ measurements can be implemented for other regions.

The information and data obtained from this study are important given current climate conditions and increasing atmospheric CO_2 concentrations; as the oceans continue to absorb CO_2, Ω_{Ar} values are expected to decrease in response to the lower availability of carbonate molecules. While large-scale trends have been established, regional trends are not as well defined and vary by location. The practice of downscaling and forcing in situ algorithms with satellite measurements has the potential to reveal the full breadth of surface ocean dynamics for smaller geographic areas.

LITERATURE CITED

Barker, S. & Ridgwell, A. (2012). Ocean acidification. *Nature Education Knowledge*. 3(10):21. https://www.nature.com/scitable/knowledge/library/ocean-acidification-25822734/.

Barkley, H.C., Halperin, A. A., Smith, J. N., Weible, R., Pomeroy, N. (2021). National Coral Reef Monitoring Program: Dissolved inorganic carbon, total alkalinity, pH and other variables collected from surface discrete measurements using Coulometer, alkalinity titrator and other instruments from the Hawaiian Archipelago, from 2019-04-21 to 2019-09-05 (NCEI Accession 0226794). Subsets 315R20190821, 330C20190419, 330C20190709, 330C20190722. NOAA National Centers for Environmental Information. Dataset. https://doi.org/10.25921/fxjn-r752. Accessed 08/10/2022.

Bakker, D. C. E., Pfeil, B., Landa, C. S., Metzl, N., O'Brien, K. M., Olsen, A., Smith, K., Cosca, C., Harasawa, S., Jones, S. D., Nakaoka, S., Nojiri, Y., Schuster, U., Steinhoff, T., Sweeney, C., Takahashi, T., Tilbrook, B., Wada, C., Wanninkhof, R., Alin, S. R., Balestrini, C. F., Barbero, L., Bates, N. R., Bianchi, A. A., Bonou, F., Boutin, J., Bozec, Y., Burger, E.F., Cai, W.-J., Castle, R. D., Chen, L., Chierici, M., Currie, K., Evans, W., Featherstone, C., Feely, R. A., Fransson, A., Goyet, C., Greenwood, N., Gregor, L., Hankin, S., Hardman-Mountford, N. J., Harlay, J., Hauck, J., Hoppema, M., Humphreys, M. P., Hunt, C. W., Huss, B., Ibánhez, J. S. P., Johannessen, T., Keeling, R., Kitidis, V., Körtzinger, A., Kozyr, A., Krasakopoulou, E., Kuwata, A., Landschützer, P., Lauvset, S. K., Lefèvre, N., Lo Monaco, C., Manke, A., Mathis, J. T., Merlivat, L., Millero, F. J., Monteiro, P. M. S., Munro, D. R., Murata, A., Newberger, T., Omar, A. M., Ono, T., Paterson, K., Pearce, D., Pierrot, D., Robbins, L. L., Saito, S., Salisbury, J., Schlitzer, R., Schneider, B., Schweitzer, R., Sieger, R., Skjelvan, I., Sullivan, K. F., Sutherland, S. C., Sutton, A. J., Tadokoro, K., Telszewski, M., Tuma, M., Van Heuven, S. M. A. C., Vandemark, D., Ward, B., Watson, A. J., and Xu, S. (2016). A multi-decade record of high-quality fCO2 data in version 3 of the Surface Ocean CO2 Atlas (SOCAT). Earth Syst. Sci. Data. 8, 383–413. https://doi.org/10.5194/essd-8-383-2016.

Chin, T. M., Vazquez-Cuervo, J., & Armstrong, E. M. (2017). A multi-scale high-resolution analysis of global sea surface temperature. *Elsevier.* Remote Sensing of Environment. 200, 154-169. https://doi.org/10.1016/j.rse.2017.07.029.

Cyronak, T., Schulz, K. G., & Jokiel, P. L. (2016). The omega myth: What really drives lower calcification rates in an acidifying ocean. *ICES Journal of Marine Science*. 73(3), 558 562. https://doi.org/10.1093/icesjms/fsv075.

Cyronak, T., Andersson, A. J., Langdon, C., Albright, R., Bates, N. R.,, Caldeira, K., Carlton, R., Corredor, J. E., Dunbar, R. B., Enochs, I., Erez, J., Eyre, B. D., Gattuso, J.-P., Gledhill, D., Kayanne, H., Kline, D. I., Koweek, D. A., Lantz, C., Lazar, B., Manzello, D., McMahon, A., Meléndez, M., Page, H. N., Page, H. N., Santos, I. R., Schulz, K. G., Shaw, E., Silverman, J., Suzuki, A., Teneva, L., Watanabe, A., & Yamamoto, S. (2018). Taking the metabolic pulse of the world's coral reefs. *PLoS ONE*. https://doi.org/10.1371/journal.pone.0190872.

Dickson, A. G., Sabine, C. L. and Christian, J. R. (Eds.) (2007). Guide to Best Practices for Ocean CO_2 Measurements. PICES Special Publication 3, 191 pp.

Doney, S. C., Busch, D. S., Cooley, S. R., & Kroeker, K. J. (2020). The impacts of ocean acidification on marine ecosystems and reliant human communities. Annual Review of Environment and Resources. https://doi.org/10.1146/annurev-environ-012320-083019.

Dunne, J. P., John, J. G., Shevliakova, E. N., Stouffer, R. J., Krasting, J. P., Malyshev, S. L., Milly, P. C. D., Sentman, L. T., Adcroft, A. J., Cooke, W., Dunne, K. A., Griffies, S. M., Hallberg, R. W., Harrison, M. J., Levy, H., Wittenberg, A. T., Phillips, P. J., & Zadeh, N. (2013). GFDL's ESM2 global coupled climate–carbon earth system models. Part II: Carbon system formulation and baseline simulation characteristics. *Journal of Climate*. 26(7), 2247-2267. https://doi.org/10.1175/JCLI-D-12-00150.1.

Franklin, E. C., P. L. Jokiel, & Donahue, M. J. (2013). Predictive modeling of coral distribution and abundance in the Hawaiian Islands. Marine Ecology Progress Series. 481: 121-132. https://doi.org/10.3354/meps10252.

Franklin, E. C., P. L. Jokiel, & Donahue, M. J. (2014). Data from: Predictive modeling of coral distribution and abundance in the Hawaiian Islands. Dryad Digital Repository. https://doi.org/10.5061/dryad.9vd0q.

Friedrich, T., Powell B. S., Veazey, L., Hahn-Woernle, L., & Stock, C. (2020). Modeling the spatio-temporal variations of ocean acidification for Hawaiian corals. Poster. Simons Foundation. University of Hawaii, Department of Oceanography. JIMAR. NOAA.

Friedrich, T., Powell, B. S., Stock, C. A., Hahn-Woernle, L., Dussin, R., & Curchitser, E. N. (2021). Drivers of phytoplankton blooms in Hawaii: A regional model study. *Journal of Geophyscial Research: Oceans*. 126, e2020jc017069. https://doi.org/10.1029/2020JC017069.

Gledhill, D. K., Wanninkhof, R., Millero F. J., & Eakin, M. (2008). Ocean acidification of the Greater Caribbean Region 1996– 2006. *Journal of Geophysical Research: Oceans*. 113, C10031. https://doi.org/10.1029/2007JC004629.

Gruber, N., Clement, D., Carter, B. R., Feely, R. A., Van Heuven, S., Hoppema, M., Ishii, M., Key, R. M., Kozyr, A., Lauvset, S. K., Lo Monaco, C., Mathis, J. T., Murata, A., Olsen, A., Perez, F. F., Sabine, C. L., Tanhua, T., & Wanninkhof, R. (2019). The oceanic sink for anthropogenic CO2 from 1994-2007. *Science*. 363, 6432, 1193-1199. https://doi.org/10.1126/science.aau5153.

Guan, Y., Hohn, S., & Merico, A. (2015). Suitable environmental ranges for potential coral reef habitats in the tropical ocean. *PLoS ONE.* https://doi.org/10/1371/journal.pone.0128831.

Guinotte, J. M., Kleypas, J., & Buddemeier, R. W. (2003). Future coral reef habitat marginality: Temporal and spatial effects of climate change in the Pacific basin. *Coral Reefs*. 22(4), 551-558. https://link.springer.com/article/10.1007/s00338-003-0331-4.

Haigh, R., Ianson, D., Holt, C. A., Neate, H. E., Edwards, A. M. (2015). Effects of ocean acidification on temperature coastal marine ecosystems and fisheries in the northeast Pacific. *PLoS ONE.* 10(2), e0117533. https://doi.org/10.1371/journal.pone.0117533.

Heinze, C., Meyer S., Goris, N., Anderson, L., Steinfeldt R., Change, N., Quéré, C. L., & Bakker, D. C. E. (2015). The ocean carbon sink – impacts, vulnerabilities and challenges. *Earth System Dynamics*. https://doi.org/10.5194/esd-6-327-2015.

Humphreys, M. P., Lewis, E. R., Sharp, J. D., and Pierrot, D. (2022). PyCO2SYS v1.8: marine carbonate system calculations in Python. *Geoscientific Model Development*. 15, 15-43. https://doi.org/10.5194/gmd-15-15-2022.

Jones, J. M., Sweet J., Brzezinski, M. A., McNair, H. M., & Passow, U. (2016). Evaluating carbonate system algorithms in a nearshore systems: does total alkalinity matter? *PLoS ONE. 11(11), e0165191*. https://doi:10.1371/jounral.pone.0165191.

JPL MUR MEaSUREs Project (2015). GHRSST Level 4 MUR Global Foundation Sea Surface Temperature Analysis. Ver. 4.1. PO.DAAC, CA, USA. Access dates vary. https://doi.org/10.5067/GHGMR-4FJ04.

Kleypas, J. A. (1995). A diagnostic model for predicted global coral reef distribution. In: Bellwood O (ed.). PACON International and James Cook University of N. Queensland. *Recent advances in marine science and technology '94*. 211-220.

Kleypas, J. A., McManus, J. W., & Meñez, L. A. B. (1999). Environmental limits to coral reef development: where do we draw the line? *Amer. Zool*. 39: 146-159.

Kleypas, J. A., Buddemeier, R. W., Archer, D., Gattuso, J.-P., Langdon, C., & Opdyke, B. N. (1999). Geochemical consequences of increased atmospheric carbon dioxide on coral reefs. *Science*. 284, 5411, 118-120. https://doi.org/10.1126/science.284.5411.118.

Kleypas, J. A., Feely, R. A., Fabry, V. J., Langdon, C., Sabine, C. L., & Robbins, L. L. (2006). Impacts of Ocean Acidification on coral reefs and other marine calcifiers: A guide for future research, report of a workshop held 18-20 April 2005, St. Petersburg, FL, sponsored by NSF; NOAA, and the U.S. Geological Survey. 88 pp.

Knor, L., Meléndez, M., Howins, N., Boeman, D., Lechner, E., DeCarlo, D., & Sabine, C. (2018). Dissolved inorganic carbon, total alkalinity, water temperature and salinity collected from surface discrete observations using coulometer, alkalinity titrator and other instruments from the coral reef MPCO2 buoys at Ala Wai, CRIMP-2, Kaneohe, and Kilo Nalu from 2016-01-08 to 2020-12-20 (NCEI Accession 0176671). All subsets used. NOAA National Centers for Environmental Information. Dataset. https://doi.org/10.25921/pe6v-qg74. Accessed 03/19/2023.

Kroeker, K. J., Kordas, R. L., Crim, R., Hendriks, I. E., Ramajo, L., Singh, G. S., Duarte, C. M., & Gattuso, J.-P. (2013). Impacts of ocean acidification on marine organisms: quantifying sensitivities and interaction with warming. *Global Change Biology*. 19, 1884-1896. https://doi.org/10.1111/gcb.12179.

Land, P. E., Shutler, J. D., Findlay, H. S., Girard-Ardhuin, F., Sabia, R., Reul, N., Piolle, J.-F., Chapron, B., Quilfen, Y., Salisbury, J., Vandemark, D., Bellerby, R., & Bhadury, P. (2015). Salinity from space unlocks satellite-based assessment of Ocean Acidification. *Environ. Sci. Technol*. 49, 1987-1994. https://doi.org/10.1021/es504849s.

Land, P. E., Findlay, H. S., Shutler, J. D., Ashton, I. G. C., Holding, T., Grouazel, A., Girard Ardhuin, F., Reul, N., Piolle, J.-F., Chapron, B., Quilfen, Y., Bellerby, R. G. J., Bhadbury, P., Salisbury, J., Vandemark, D., & Saba, R. (2019). Optimum satellite remote sensing of

the marine carbonate system using empirical algorithms in the global ocean, the Greater Caribbean, the Amazon Plume and the Bay of Bengal. *ScienceDirect*. 235. https://doi.org/10.1016/j.rse.2019.111469.

Lauvset, S. K., Lange, N., Tanhua, R., Bittig, H. C., Olsen, A., Kozyr, A., Alin, S. R., Álvarez, M., Azetsu-Scott, K., Barbero, L., Becker, S., Brown, P. J., Carter B. R., Cotrim da Cunha, L., Feely, R. A., Hoppema, M., Humphreys, M. P., Ishii, M., Jeansson, E., Jiang, L. Q., Jones, S. D., Lo Monaco, C., Murata, A., Müller, J. D., Pérez, F. F., Pfeil, B., Schirnick, C., Steinfeldt R., Suzuki, R., Tilbrook, B., Ulfsbo, A., Velo A., Woosley, R. J., and Key, R. M. (2022). GLODAPv2.2022: the latest version of the global interior ocean biogeochemical data product. *Earth Syst. Sci*. Data Discuss., 2022, 1-37. https://doi.org/10.5194/essd-2022-293.

Lauvset, S. K., Lange, N., Tanhua, T., Bittig, H. C., Olsen, A., Kozyr, A., Álvarez, M., Becker, S., Brown, P. J., Carter, B. R., Cotrim da Cunha, L., Feely, R. A., Van Heuven, S., Hoppema, M., Ishii, M., Jeansson, E., Jutterström, S., Jones, S. D., Karlsen, M. K., Lo Monaco, C., Michaelis, P., Murata A., Pérez, F. F., Pfeil, B., Schirnick, C., Steinfeldt, R., Suzuki, R., Tilbrook, B., Velo, A., Wanninkhof, R., Woosley, R. J. & Key, R. M. (2021). An updated version of the global interior ocean biogeochemical data product, GLODAPv2.2021. *Earth Syst. Sci*. Data, 13, 5565-5589. https://doi.org/10.5194/essd-13-5565-2021.

Lee, K., Tong, L. T., Millero, F. J., Sabine, C. L., Dickson, A. G., Goyet, C., Park, G.-H., Wanninkhof, R., Feely, R. A., & Key, R. M. (2006). Global relationships of total alkalinity with salinity and temperature in surface waters of the world's oceans. *Geophysical Research Letters*. https://doi.org/10.1029/2006GL027207.

Lohrenze, S. E., Cai W.-J., Chakraborty, S., Huang, W.-J., Guo X., He, R., Xue Z., Fennel K.,

Howden, S., Tian, H. (2018). Satellite estimation of coastal pCO2 and air-sea flux of carbon dioxide in the northern Gulf of Mexico. *Elsevier*. Remote Sensing of Environment. 207, 71-83. https://doi.org/10.1016/j.rse.2017.12.039.

Loke, M. K., Geslani, C., Takenaka, B., & Leung, P. (2015). Seafood consumption and supply sources in Hawaii, 2000-2009. *Marine Fisheries Review*. 74(4), 44-51.

Meissner, T., Wentz, F. J., Manaster, A., & Lindsley, R. (2019). Remote sensing systems SMAP ocean surface salinities [Level 2C, Level 3 Running 8-day, Level 3 Monthly], version 4.0 validated release. Remote sensing systems, Santa Rosa, CA, USA. Available online at www.remss.com/missions/smap. https://doi.org/10.5067/smp40-3smcs.

Melnichenko, O., Hacker, P., Maximenko, N., Lagerloef, G., & Potemra, J. (2016). Optimum interpolation analysis of Aquarius sea surface salinity. *Journal of Geophysical Research: Oceans*. 121, 602-616. https://doi.org/10.1002/2015JC011343.

Melnichenko, O., Hacker, P., Potemra J., Meissner, T., & Wentz, F. (2021). Aquarius/SMAP sea surface salinity optimum interpolation analysis. IPRC Technical Note No. 7, May 7, 2021. https://doi.org/10.5067/SMP10-4U7CS.

Millero, F., Lee, K., & Roche, M. (1998). Distribution of alkalinity in the surface waters of the major oceans. *Marine Chemistry*. 60, 111-130. https://doi.10.1016/S0304-4203(97)00084-4.

Olsen, A., Key, R. M., Van Heuven, S., Lauvset, S. K., Velo, A., Lin, X., Schirnick, C., Kozyr, A., Tanhua, T., Hoppema, M., Jutterström, S., Steinfeldt, R., Jeansson, E., Ishii, M., Pérez, F. F., & Suzuki, T. (2016). The Global Ocean Data Analysis Project version 2 (GLODAPv2) – an internally consistent data product for the world ocean. *Copernicus Publications*. 8, 297-323. https://doi.org/10.5194/essd-8-297-2016.

Pidcock, R. (2015). Ocean acidification: new satellite reveals places on Earth most at risk from Ocean Acidification. https://www.carbonbrief.org/new-satellite-reveals-places-on-earth-most-at-risk-from-ocean-acidification.

Powell, B. S. (2017). Quantifying how observations inform a numerical reanalysis of Hawaii. *Journal of Geophysical Research: Oceans*. 122, 8427-8444. https://doi.org/10.1002/2017JC012854.

Shamberger, K. E. F., Feely, R. A., Sabine, C. L., Atkinson, M. J., DeCarlo, E. H., Mackenzie, F. T., Drupp, P. S., & Butterfield, D. A. (2011). *Elsevier*. Marine Chemistry. 127, 64-75. https://doi.org/10.1016/j.marchem.2011.08.003.

Scholey, V., Bromhead, D., Margulies, D., Nicol, S., Wexler, J., Santiago, M., Williamson, J. E., Hoyle, S., Schlegel, P., Havenhand, J., Ilyina, T., & Lehodey, P. (2012). Novel research into the impacts of Ocean Acidification upon tropical tuna. University of Hawaii at Manoa. *Pelagic Fisheries Research Program*. 16, 1.

Takahashi, T., Sutherland, S. C., Sweeney, C., Poisson, A., Metzl, N., Tilbrook, B., Bates, N., Wanninkhof, R., Feely, R. A., Sabine, C., Olafsson, J., & Nojiri, Y. (2002). Global sea-air CO_2 flux based on climatological surface ocean pCO_2, and seasonal biological and temperature effects. *Elsevier.* Deep Sea Research Part II: Topical Studies in Oceanography. 49, 9-10, 1601-1622. https://doi.org/10.149016/S0967-0645(02)00003-6.

Weiss, R. F. (1974). Carbon dioxide in water and seawater: the solubility of a non-ideal gas. Scripps Institution of Oceanography. *Marine Chemistry*. 2:203-215.

Weiss, R. F. and Price, B. A. (1980). Nitrous oxide solubility in water and seawater. *Marine Chemistry*. 8:347-359.